Combustion Theory and Modelling, 2016
Vol. 20, No. 1, 1–33, http://dx.doi.org/10.1080/13647830.2015.1114148

Flame balls in non-uniform mixtures: existence and finite activation energy effects

Remi Daou[a], Philip Pearce[b] and Joel Daou[b*]

[a]*Faculté d'ingénierie-ESIB, Université Saint-Joseph, Lebanon;* [b]*School of Mathematics, University of Manchester, Manchester, UK*

(*Received 17 July 2015; accepted 18 October 2015*)

The paper's broad motivation, shared by a recent theoretical investigation [Daou and Daou, "Flame balls in mixing layers," *Combustion and Flame*, Vol. 161 (2014), pp. 2015–2024], is a fundamental but apparently untouched combustion question; specifically, 'What are the critical conditions insuring the successful ignition of a diffusion flame by means of an external energy deposit (spark), after mixing of cold reactants has occurred in a mixing layer?' The approach is based on a generalisation of the concept of Zeldovich flame balls, well known in premixed reactive mixtures, to non-uniform mixtures. This generalisation leads to a *free boundary problem* (FBP) for axisymmetric flame balls in a two-dimensional mixing layer in the distinguished limit $\beta \to \infty$ with $\epsilon_L = O(1)$; here β is the Zeldovich number and ϵ_L is a non-dimensional measure of the stoichiometric premixed flame thickness. The *existence of such flame balls is the main object of current investigation*. Several original contributions are presented. First, an analytical contribution is made by carrying out the analysis of Daou and Daou (2014) in the asymptotic limit $\epsilon_L \to 0$ to higher order. The results capture, in particular, the dependence of the location of the flame ball centre (argued to represent the optimal ignition location which differs from the stoichiometric location) on ϵ_L. Second, two detailed numerical studies of the axisymmetric flame balls are presented for arbitrary values of ϵ_L. The first study addresses the infinite-β FBP and the second one the original finite-β problem based on the constant density reaction–diffusion equations. In particular, it is shown that solutions to the FBP exist for arbitrary values of ϵ_L while actual finite-β flame balls exist in a specific domain of the β–ϵ_L plane, namely for ϵ_L less than a maximum value proportional to $\sqrt{\beta}$; this scaling is consistent with the existence of solutions to the FBP for arbitrary ϵ_L. In fact, the flame ball existence domain is found to have little dependence on the stoichiometry of the reaction and to coincide, to a good approximation, with the domain of existence of the positively-propagating two-dimensional triple flames in the mixing layer. Finally, we confirm that the flame balls are typically unstable, as one expects in the absence of heat losses.

Keywords: flame balls; forced ignition of diffusion flame; ignition in non-uniform mixtures

1. Introduction

In order to understand the problem of successful flame ignition in a non-uniform reactive mixture, typically exemplified by a localised energy deposit leading to triple flame propagation and the establishment of a diffusion flame in a mixing layer, a theoretical study has been recently published which seems to be the only analytical investigation in the literature [1]. The present paper is a continuation of this investigation and it shares with it the broad motivation of understanding a fundamental problem which is important

*Corresponding author. Email: joel.daou@manchester.ac.uk

in applications. This is the problem of the forced ignition of a diffusion flame, by means of a spark say, after the mixing of cold reactants has occurred resulting in the formation of a mixing layer. Surprisingly, this fundamental problem, concerned for example with the determination of the minimum ignition energy required for ignition and the optimal location for its deposit, has not received, to our knowledge, dedicated attention in the literature.

An important objective of [1] was to determine the critical minimum ignition energy which was argued to be, in first approximation, the thermal energy inside a non-propagating non-spherical axisymmetric structure, called a flame ball, generalising the well-known spherical Zeldovich flame ball to non-uniform mixtures. This stationary axiymmetric structure is expected to be unstable, as is the case with its spherical counterpart in uniform premixed gases [2, p. 327], except in special circumstances where preferential diffusion and volumetric heat losses are taken into account [3–6]. However, the instability of flame balls does not in any way diminish their importance. On the contrary, their instability may be viewed as an essential ingredient for characterising the 'critical conditions' for successful ignition in a first theoretical analysis of flame initiation in non-uniform reactive mixtures. This interpretation is in line with Zeldovich's pioneering interpretation of such stationary unstable structures in (perfectly) premixed gases as described by the following quotation [2, p. 331]: 'This type of stationary combustion at a spherical surface could be viewed as the condition that must be overcome in order to ignite a gas, i.e., in order to produce a uniformly propagating combustion wave. If a thermal source with the same temperature, but a smaller radius, is created in a reactive gas, then the source will be dissipated. On the other hand, if the radius of a source with the same temperature exceeds the radius of the sphere, then ignition occurs'.

The short discussion above provides one significant motivation, related to ignition in non-uniform mixtures, for the study of stationary axisymmetric flame balls. In this ignition context, two important questions arise, namely 'What is the minimum energy (of a spark say) required for ignition?' and 'What is the optimal location in the mixing layer for energy deposition?' Answers to these two questions may be related to the thermal-energy content of the flame ball and to its location, which are both fixed by the parameters of the problem. We note that the question related to the location is not relevant to the case of uniform premixed gases, but is fundamental in our non-uniform case. In fact, it is not generally true that the optimal location should coincide with the stoichiometric location, as an educated guess may suggest, but as we shall see, this location is mainly determined by the stoichiometry of the reaction and the Damköhler number. We shall not repeat herein the introductory remarks given in reference [1] to further motivate this study. The interested reader is referred to this publication for this purpose, as well as for a discussion of the most relevant references related both to flame balls and to triple flames (which will be involved in the interpretation of results, e.g. those associated with the existence of the flame balls and their location). We find it important however to underline a few key points from [1] which help set the objectives of the current investigation. In particular, we note that the constant density model used in [1], describing axisymmetric flame balls in a two-dimensional mixing layer, will be adopted here. As we shall discuss in Section 2, the model leads to a non-dimensional problem involving six parameters, which we shall refer to throughout as the *finite-β problem* to distinguish it from the *free boundary problem* (FBP) introduced below. The focus of the current investigation is restricted to three of the six non-dimensional parameters, namely β, ϵ_L and Δ; these are defined in the next section and represent the Zeldovich number, the planar stoichiometric flame thickness[1] and the stoichiometry of the reaction, respectively.

In the distinguished limit $\beta \to \infty$ with $\epsilon_L = O(1)$, the *finite-β problem* was shown in [1] to lead to a *free boundary problem*. The FBP was solved analytically by perturbation methods

in the (fast-chemistry or large-Damköhler) limit $\epsilon_L \to 0$. The FBP and the corresponding analytical formulae are summarised and discussed in Sections 3.1 and 3.2. These formulae determine in particular the flame ball shape and the corresponding thermal energy (argued to represent the minimum ignition energy) for small values of ϵ_L. It is important to emphasise that no information is available about the solutions to the FBP for arbitrary values of ϵ_L. In fact, the very existence of such solutions is not guaranteed and requires examination. Therefore, numerical calculations are needed to this end, as well as to check the validity of the asymptotics for small values of ϵ_L. Similarly, the solutions to the finite-β problem and their existence need also be examined and furthermore compared with those of the FBP. These remarks determine the **main objectives** of the current paper, which are:

(a) to test the validity of the asymptotic findings of [1] by comparing them with numerical solutions to (i) the FBP and (ii) the finite-β problem;
(b) to determine the flame ball's existence domain in the β–ϵ_L plane as solutions to the finite-β problem, as well as their ϵ_L-domain of existence as solutions to the FBP – this is crucial information without which the theory would have shaky foundations;
(c) to determine the influence of the stoichiometric coefficient Δ on the results;
(d) to determine the dependence of the location around which the flame ball must be centred (for it to exist) on ϵ_L both analytically, for small values of ϵ_L, and numerically in the general case – this location is important as it may be argued to represent the optimal location for energy deposition.

The numerical results, as well as additional new analytical results, to be presented should provide crucial information completing the theory of [1], e.g. regarding the existence of the flame ball solutions, and a fairly thorough appreciation of the dependence of the flame balls on the physical parameters considered.

The paper is carefully written and essential details are provided with some necessary partial repetitions from [1], including a summary of its main findings, in order to insure clarity. Some effort is required in reading the paper, however, given the intricacies of the problem. These intricacies are associated with the required links to several theoretical aspects of combustion (the asymptotics of triple flames, flame balls, diffusion flames, and distinguished limits related to the presence of *four spatial scales* – see Figure 1 and its captions, to be introduced shortly). The level of detail adopted in the presentation is hence deemed necessary in order to facilitate understanding and benefit future workers on this rich topic (rather than merely listing new results which are far from obvious).

The paper is structured as follows. We begin in Section 2 by formulating the problem and defining the scope of the study. The FBP is presented in Section 3.1 and the corresponding analytical results from [1] are summarised and discussed in Section 3.2. These are followed by new asymptotic results whose derivation is motivated and presented in Section 3.3. The numerical simulations pertaining to the FBP are addressed in Section 4 and those pertaining to the finite-β problem in Section 5. The paper closes with concluding remarks, summarising and discussing the main findings, and with suggestions for future investigations. These investigations should include the combined study of preferential diffusion, heat losses, and the stability of flame balls; stability is addressed in Section 5.6 only in passing and is restricted to an equidiffusional adiabatic context to illustrate the generic situation, important for ignition, where the flame ball is unstable. Additional topics for future studies addressing aspects which are important in practice, such as the effect of variable density and the relation between successful ignition and spark duration (as described in [7] for a premixed gas), are not considered in this paper. This exclusion is adopted intentionally in order to

allow a proper treatment addressing the main objectives listed above, mostly related to the existence of flame balls. The extensive set of results thus obtained present however a significant addition to the theory and should provide a useful benchmark for comparison with future studies.

2. Formulation

The setup for the investigation of flame balls in a mixing layer is the same as the one adopted in [1]. Namely, we consider a reactive mixture in a two-dimensional channel delimited by two planes located at $Z = \pm L$ as depicted in Figure 1. The planes represent two porous walls where the concentrations of the fuel F and oxidiser O are assumed to be maintained fixed. Although this setup may be difficult to achieve experimentally, it is adopted here to construct the simplest theoretical model for an axisymmetric flame ball as depicted in the left half of the figure; this is a non-propagating structure of burnt gas, axisymmetric with respect to the vertical Z-axis, which is surrounded by an unburnt mixture of infinite extent in the horizontal X- and Y-directions. A similar setup has been used in several previous investigations (see e.g. [8–11]) which addressed, in particular, the propagation of 2D triple flames and the buoyancy-induced instability of 1D diffusion flames; these 2D and 1D combustion structures, which will enter the discussion at several points of the text, are represented in the right half of the figure.[2] Extension of the study to other slightly

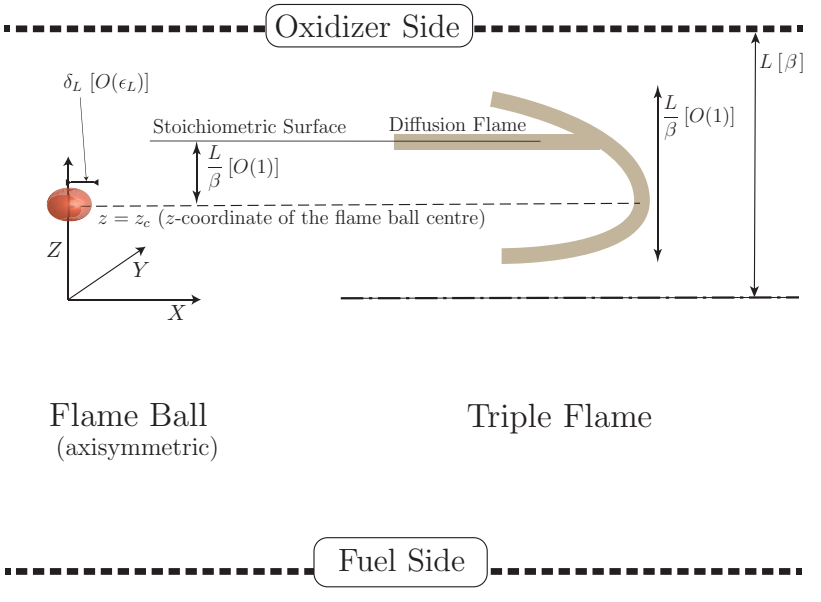

Figure 1. A flame ball in a non-uniform reactive mixture between two porous walls (left half of the figure) and a triple flame (right half). The mass fractions are prescribed by $Y_F = Y_{F,F}$ and $Y_O = 0$ on the fuel side, and $Y_F = 0$ and $Y_O = Y_{O,O}$ on the oxidiser side. Non-dimensional length scales introduced in the text are enclosed in square brackets. Note that the z-coordinate of the flame ball centre is depicted as coinciding with the z-coordinate of the leading edge of the triple flame; this is justified by the asymptotic analysis of [1]. Note that four scales are present in our flame ball problem: L, L/β, δ_L and δ_L/β, describing respectively the vertical size of the domain, the location of the flame ball centre, the size of the flame ball, and the thickness of the reaction zone around the flame ball. The corresponding non-dimensional scales are β, 1, ϵ_L and ϵ_L/β.

more complex setups, probably easier to realise experimentally, such as the axisymmetric counterflow configuration adopted in [12], will be the subject of future investigations.

The combustion is represented by a one-step reaction of the form

$$\mathrm{F} + s\mathrm{O} \rightarrow (1+s)\mathrm{Product} + q,$$

where s and q denote the mass of oxidiser consumed and the heat released per unit mass of fuel. The reaction rate $\tilde{\omega}$, defined as the mass of fuel consumed per unit volume and unit time, is assumed to obey an Arrhenius law with pre-exponential factor B and activation energy E of the form

$$\tilde{\omega} = B\rho^2 Y_\mathrm{F} Y_\mathrm{O} \exp(-E/RT). \tag{1}$$

Here ρ, Y_F, Y_O, R and T represent the density, the fuel mass fraction, the oxidiser mass fraction, the universal gas constant and the temperature, respectively.

For large activation energies, the region which is able to sustain significant heat generation is centred around the stoichiometric surface where $Y_\mathrm{O} = sY_\mathrm{F}$. In the frozen mixture far away from the flame ball, i.e. for $X^2 + Y^2 \rightarrow \infty$, this surface is located at $Z = Z_\mathrm{st}$ which is determined using the mass fractions profiles which are linear in Z there. Specifically, we have

$$\frac{Z_\mathrm{st}}{L} = \Delta \equiv \frac{S-1}{S+1}, \tag{2}$$

where $S \equiv sY_{\mathrm{F,\,F}}/Y_{\mathrm{O,\,O}}$ is a normalized stoichiometric coefficient and Δ a scaled version thereof which we shall use instead.

Note that the location of the stoichiometric surface is midway between the walls, i.e. $Z_\mathrm{st} = 0$, if the conditions are such that $\Delta = 0$ (or $S = 1$), a special case which we shall refer to as the stoichiometrically balanced case; in this special case, the flame balls exist only if centred at the stoichiometric surface. *In the general case $\Delta \neq 0$, the flame ball centre is located away from the stoichiometric surface, at a distance of order L/β as indicated in the figure*.[3] In fact $\Delta > 0$ in this specific figure, hence the stoichiometric surface and the flame ball centre are located closer to the oxidiser boundary; their locations would be closer to the fuel boundary if $\Delta < 0$.

With the subscript 'st' indicating values at $(X^2 + Y^2) \rightarrow \infty$, $Z = Z_\mathrm{st}$, we introduce the scaled quantities

$$y_\mathrm{F} = \frac{Y_\mathrm{F}}{Y_{\mathrm{F,\,st}}}, \quad y_\mathrm{O} = \frac{Y_\mathrm{O}}{Y_{\mathrm{O,\,st}}}, \quad \theta = \frac{T - T_u}{T_\mathrm{ad} - T_u}.$$

Here $T_\mathrm{ad} \equiv T_u + qY_{\mathrm{F,\,st}}/c_p$ is the adiabatic flame temperature, which is used to define the Zeldovich number $\beta \equiv E(T_\mathrm{ad} - T_u)/RT_\mathrm{ad}^2$ at the conditions prevailing at the stoichiometric location. At these conditions (and for $\beta \gg 1$), the laminar speed S_L of the stoichiometric planar flame with thickness $\delta_L \equiv D_T/S_L$ is given by

$$S_L = \sqrt{\frac{4\mathrm{Le_F Le_O}}{\beta^3} Y_{\mathrm{O,\,st}} (\rho D_T) B \exp(-E/RT_\mathrm{ad})}, \tag{3}$$

where D_T, $\mathrm{Le_F}$ and $\mathrm{Le_O}$ are the thermal diffusivity, the fuel Lewis number and the oxidiser Lewis number, respectively.

The non-dimensional equations are given by

$$\frac{\partial\theta}{\partial t} = \nabla^2\theta + \epsilon_L^{-2}\omega \tag{4a}$$

$$\frac{\partial y_\mathrm{F}}{\partial t} = \mathrm{Le_F^{-1}}\nabla^2 y_\mathrm{F} - \epsilon_L^{-2}\omega \tag{4b}$$

$$\frac{\partial y_\mathrm{O}}{\partial t} = \mathrm{Le_O^{-1}}\nabla^2 y_\mathrm{O} - \epsilon_L^{-2}\omega, \tag{4c}$$

in terms of the coordinates

$$x = \frac{\beta X}{L}, \quad y = \frac{\beta Y}{L}, \quad z = \frac{\beta(Z - Z_\mathrm{st})}{L}, \tag{5}$$

after selecting $L_r \equiv L/\beta$ as unit length and L_r^2/D_T as unit time.[4] As discussed in [1], L_r represents the appropriate scale for measuring the radius of curvature of the triple flame (sketched in the figure) which can propagate in the mixing layer, as well as for measuring the distance between the location where the flame balls are centred and the stoichiometric surface. As for the parameter ϵ_L, it represents the thickness of the planar stoichiometric flame measured with the reference length L/β; it is also related to the Damköhler number Da defined as the ratio between the diffusion time across the mixing layer L^2/D_T and the flame transit time δ_L^2/D_T. Specifically, we have

$$\epsilon_L \equiv \frac{\delta_L}{L_r} = \frac{\beta D_T}{L S_L} \quad \text{and} \quad \mathrm{Da} \equiv \frac{L^2}{\delta_L^2} = \beta^2\epsilon_L^{-2}. \tag{6}$$

The non-dimensional reaction rate ω takes the form

$$\omega = \frac{\beta^3}{4\mathrm{Le_F Le_O}} y_\mathrm{F} y_\mathrm{O} \exp\left[\frac{\beta(\theta-1)}{1+\alpha(\theta-1)}\right], \tag{7}$$

where $\alpha = (T_\mathrm{ad} - T_u)/T_\mathrm{ad}$.

The boundary conditions, corresponding to frozen profiles in the far field and prescribed values on the walls, are

$$\theta = 0 \tag{8a}$$

$$y_\mathrm{F} = 1 - \frac{z}{\beta(1-\Delta)} \tag{8b}$$

$$y_\mathrm{O} = 1 + \frac{z}{\beta(1+\Delta)}, \quad \text{as} \quad x^2 + y^2 \to \infty,\ z \to -\beta(1+\Delta) \text{ or } z \to \beta(1-\Delta). \tag{8c}$$

Equations (4) with the boundary conditions (8) complete the formulation of the problem (subject to suitable initial conditions). A main aim when tackling this problem is to find its stationary solutions (flame balls) and examine their stability. In particular, one would like to determine the domain of existence of these stationary solutions, and the corresponding profiles of θ, y_F and y_O, in terms of the parameters ϵ_L, Δ, β, $\mathrm{Le_F}$, $\mathrm{Le_O}$ and α. The analysis

of these equations in the asymptotic limit $\beta \to \infty$ leads to an FBP that can be solved analytically for small values of ϵ_L; the FBP is presented in the next section along with a summary and a discussion of the main findings of [1]. This discussion will motivate more clearly the direct objectives of the paper announced in the introduction, and facilitate understanding the new results. These include the extension of the small ϵ_L asymptotic analysis to higher order, undertaken in Section 3.3, and the determination of the solutions of the infinite-β FBP and those of the finite-β problem, carried out numerically for arbitrary values of ϵ_L in Sections 4 and 5, respectively.[5]

Before proceeding, we point out that, out of the six parameters listed above, only the influence of the first three, namely ϵ_L, Δ and β, will be investigated; unless otherwise stated, the other parameters will be assigned fixed values, namely $\mathrm{Le_F} = 1$, $\mathrm{Le_O} = 1$ and $\alpha = 0.85$. Our main focus will be on the determination of the stationary solutions and their existence domains as well as on the validation of the asymptotic results. Furthermore, the instability of the flame balls in our equidiffusional adiabatic framework will be confirmed numerically rather concisely, leaving a detailed stability analysis, including differential diffusion and heat losses, for a future investigation.

3. The free boundary problem for flame balls in the limit $\beta \to \infty$

3.1. *The free boundary problem*

In the limit $\beta \to \infty$, stationary solutions of Equations (4a)–(4c) with the boundary conditions (8), representing flame balls in the mixing layer, are solutions of an FBP. This FBP has been derived in [1] in the distinguished limit $\beta \to \infty$ with ϵ_L, l_F, $l_\mathrm{O} = \mathcal{O}(1)$, where $l_\mathrm{F} \equiv \beta(\mathrm{Le_F} - 1)$ and $l_\mathrm{O} \equiv \beta(\mathrm{Le_O} - 1)$ are the reduced Lewis numbers. It consists of a single Laplace equation for *the leading order temperature denoted by* ψ to be solved outside a domain Ω (the burnt gas domain), with ψ required to vanish in the far field and to satisfy two conditions on the unknown boundary $\partial\Omega$ of Ω (the infinitely thin reaction sheet):

$$\nabla^2\psi = 0 \qquad \text{in } R^3\backslash\Omega \tag{9a}$$

$$\psi = 0, \qquad \text{as } |\mathbf{r}| \to \infty \tag{9b}$$

$$\psi = 1, \quad \frac{\partial\psi}{\partial n} = -\overline{\mathcal{F}} \qquad \text{on } \partial\Omega. \tag{9c}$$

Here $\overline{\mathcal{F}}$ is an explicit function of $(z; \epsilon_L, \Delta, l_\mathrm{F}, l_\mathrm{O})$ given by

$$\overline{\mathcal{F}} = \epsilon_L^{-1}\left\{1 + \left|\frac{l_\mathrm{F} - l_\mathrm{O}}{2} + \frac{z}{1-\Delta^2}\right|\right\}^{1/2} \exp\left\{\frac{-l_\mathrm{F} - l_\mathrm{O}}{4} - \frac{\Delta z}{2(1-\Delta^2)} - \left|\frac{l_\mathrm{F} - l_\mathrm{O}}{4} + \frac{z}{2(1-\Delta^2)}\right|\right\}.$$

A significant simplification is obtained if we assume that $l_\mathrm{F} = l_\mathrm{O}$, equal to l, say, leading to

$$\overline{\mathcal{F}} = \epsilon_L^{-1} \exp\left(-\frac{l}{2}\right) \mathcal{F}(z; \Delta), \tag{10}$$

where

$$\mathcal{F} = \left\{1 + \frac{|z|}{1-\Delta^2}\right\}^{1/2} \exp\left\{-\frac{\Delta z + |z|}{2(1-\Delta^2)}\right\}. \tag{11}$$

For simplicity, we shall write in the remainder of the paper $\mathcal{F}(z)$ for $\mathcal{F}(z;\Delta)$. Also, before proceeding, we note that formulae (9)–(11) may be viewed as a generalisation of the so-called near-equidiffusion flame (NEF) approximation of premixed combustion [13, p. 39] to the specific case of flame-balls in our non-uniform mixture. This generalisation is derived in [1] and it involves jump conditions across a reaction sheet which can be obtained following the methodology of [14]. These jump conditions lead in particular to (9 c) involving the explicit function $\overline{\mathcal{F}}$.

3.2. *Summary and discussion of main analytical results*

For small values of ϵ_L, an analytical description of the solutions of the FBP (9)–(11) was recently presented in [1]. Here we summarise and discuss the main results of this publication which are needed for this investigation; we also introduce some notation that is important throughout the text. The analytical results will be complemented in the next section by the derivation of additional ones. It is shown in [1] that a flame ball can exist only if it is centred at a single location z_c of the symmetry axis; to leading order $z_c \sim z_0$ where z_0 is fully specified by the stoichiometric coefficient Δ as

$$z_c \sim z_0 = -\Delta(1 + |\Delta|). \tag{12}$$

In fact, z_0 is determined as an eigenvalue and it is found to correspond to the location of the maximum of the function $\mathcal{F}(z)$ given in (11), which also coincides with that of the leading-edge of the triple flame in the mixing layer. Furthermore, z_0 is used to define a small expansion parameter ϵ, a rescaled version of ϵ_L, as

$$\epsilon = \frac{\epsilon_L}{\mathcal{F}(z_0)} \exp\frac{l}{2}. \tag{13}$$

The perturbation approach for small ϵ leads to the following two-term expansions:

$$\psi = \frac{1}{r} + \frac{b\,\epsilon^2}{3}\left(\frac{1}{r} + \frac{1}{r^3} - \frac{3\cos^2\theta}{r^3}\right) \tag{14}$$

$$R = 1 + \frac{b\,\epsilon^2}{3}\left(2 - 3\cos^2\theta\right) \tag{15}$$

$$V = \frac{4\pi}{3}\left(1 + b\,\epsilon^2\right) \tag{16}$$

$$\frac{E_B}{E_Z} = \frac{1}{\mathcal{F}_0^3}\left(1 + b\,\epsilon^2\right), \tag{17}$$

where

$$\mathcal{F}_0 \equiv \mathcal{F}(z_0) = \frac{\exp\left(-|\Delta|/2\right)}{(1-|\Delta|)^{1/2}} \quad \text{and} \quad b = \frac{1}{4\,(1+|\Delta|)^2}. \tag{18}$$

These expressions are obtained after rewriting the problem, as explicitly given in Section 4.1, in terms of spherical coordinates centred at $(x, y, z) = (0, 0, z_c)$ and rescaled such that

$$(x, y, z - z_c) = \epsilon(r \sin\theta \cos\phi, r \sin\theta \sin\phi, r \cos\theta). \tag{19}$$

The expansions describe axisymmetric solutions (independent of the azimuthal angle ϕ) where $r = R(\theta)$ represents the domain boundary $\partial\Omega$ and ψ the temperature field for $r > R(\theta)$, i.e. outside the burnt gas region. The latter has a non-dimensional volume V and a dimensional volume $V_B = 3VV_Z/4\pi\mathcal{F}_0^3$; here $V_Z = 4\pi\delta_Z^3/3$ is the volume of the (spherical) Zeldovich flame ball at the stoichiometric location $z = 0$, whose radius $\delta_Z = \delta_L \exp(l/2)$. The thermal energies inside V_B and V_Z are denoted by E_B and E_Z, respectively; these are given by $E_B = \rho c_p(T_{\rm ad} - T_u)V_B$ and $E_Z = \rho c_p(T_{\rm ad} - T_u)V_Z$, where c_p is the heat capacity, when non-dimensional temperature variations of order β^{-1} are neglected.

In order to appreciate the meaning of the analytical findings better, and facilitate comparison with the numerical results, a few comments are in order. To this end, it is convenient to denote by ZFB(z) the (spherical) Zeldovich flame ball in a uniform mixture at the conditions prevailing at z. As argued in [1], the dimensional radius of ZFB(z) is given by $\delta_Z/\mathcal{F}(z)$. Therefore, the Zeldovich flame ball with the smallest radius, equal to $\delta_Z/\mathcal{F}_0$, is encountered at $z = z_0$, since z_0 is the maximum of $\mathcal{F}(z)$. It follows, on referring to (13) and (6), that the parameter ϵ has a simple interpretation: it is a non-dimensional measure of this minimum radius in terms of the reference length $L_r \equiv L/\beta$. Furthermore, the rescaling of the spherical coordinate system introduced in (19) is then seen to be equivalent to selecting as unit length $\delta_Z/\mathcal{F}_0$ instead of L_r; however, the scale L_r is still needed for the determination of the location z_0 used in (19) to centre the spherical coordinate system. Also needed is the mixing-layer scale L which is used in (2) for determining the stoichiometric location $\bar{z}_{\rm st} \equiv Z_{\rm st}/L$ by

$$\bar{z}_{\rm st} = \Delta. \tag{20}$$

Note that we use bars here and elsewhere to indicate that a coordinate is made non-dimensional using L as reference length, as explained in the footnote following Equation (5). In particular, the location of the flame ball centre measured with L is given by

$$\bar{z}_c = \bar{z}_{\rm st} + \frac{z_c}{\beta}, \tag{21}$$

and hence, to leading order by

$$\bar{z}_0 = \bar{z}_{\rm st} + \frac{z_0}{\beta}, \tag{22}$$

that is, using (12) and (20),

$$\bar{z}_0 = \Delta - \frac{\Delta(1 + |\Delta|)}{\beta}. \tag{23}$$

Furthermore, we shall define for future reference the maximum radius of the flame ball, $R_{\rm max}$, as the maximum of $R(\theta)$ for $0 \le \theta \le \pi$. According to (15), $R(\theta)$ is symmetric to

$O(\epsilon^2)$ with respect to the plane $\theta = \pi/2$, where the maximum is taken with

$$R_{\max} \equiv R\left(\frac{\pi}{2}\right) \sim 1 + \frac{\epsilon^2}{6\,(1+|\Delta|)^2}. \tag{24}$$

Similarly, (15) implies that $R(\theta)$ takes its minimum value $R_{\min}$ on the z-axis, $\theta = 0$ or π, with

$$R_{\min} \sim 1 - \frac{\epsilon^2}{12\,(1+|\Delta|)^2}. \tag{25}$$

Equation (25) indicates that the flame ball is deflated (flattened) on the z-axis, with the deflation increasing with ϵ, leading to flame breakup ($R_{\min} = 0$) for $\epsilon = \epsilon^*$ with

$$\epsilon^* = 2\sqrt{3}\,(1+|\Delta|)\,. \tag{26}$$

However, the conclusion concerning flame breakup, based on our small-ϵ asymptotic analysis, is questionable and is one of the points which need to be tested by solving the problem numerically. In fact, for $\epsilon = \epsilon^*$ the second term on the right of (25) becomes of the same order of magnitude as the first, suggesting that the expansion becomes invalid (which is also true for the other expansions). Therefore, the most optimistic estimate consists in identifying the ϵ-domain of validity of the asymptotics with the interval $[0, \epsilon^*]$. According to (26) the size of this interval increases with $|\Delta|$; this suggests that the predictions based on the asymptotic formulae should be more robust for higher values of $|\Delta|$. Of course, the degree of accuracy of these conclusions need again to be assessed numerically.

3.3. *Asymptotic results to higher order*

We note that the two-term asymptotic expansions (14)–(17) are obtained by solving the perturbation problem to $O(\epsilon^2)$, but this does not determine a two-term expansion for the flame ball centre z_c; this is only determined to leading order by Equation (12) which does not describe its variations with ϵ. In order to understand how z_c varies with ϵ and compare with the numerical results, a two-term expansion for z_c is needed. This two-term expansion for z_c can be obtained by solving the problem to $O(\epsilon^3)$, which provides as a bonus 3-term expansions for ψ and R. We briefly outline the main steps of the derivation. We begin by adding an additional term to each of the available expansions (12), (14) and (15) by writing

$$\begin{aligned} z_c &\sim -\Delta(1+|\Delta|) + \epsilon^2\zeta \\ \psi &\sim \frac{1}{r} + \frac{b\,\epsilon^2}{3}\left(\frac{1}{r} + \frac{1}{r^3} - \frac{3\cos^2\theta}{r^3}\right) + \epsilon^3\psi_3 \\ R &\sim 1 + \frac{b\,\epsilon^2}{3}\left(2 - 3\cos^2\theta\right) + \epsilon^3 R_3. \end{aligned}$$

Inserting these into the governing Equations (9) and following closely the methodology of [1] leads in the end to the problem

$$\nabla^2\psi_3 = 0 \qquad (r > 1) \tag{27}$$

$$\psi_3 = 0 \quad \text{as } r \to \infty \tag{28}$$

$$\frac{\partial\psi_3}{\partial r} + 2\psi_3 = 2b\zeta\cos\theta - c\cos^3\theta \quad \text{at } r = 1 \tag{29}$$

$$R_3 = \psi_3(r = 1), \tag{30}$$

where b is given by (18) and where c is defined and evaluated by

$$c \equiv \frac{\mathcal{F}_{zzz}(z_0)}{6\mathcal{F}(z_0)} = \begin{cases} -\dfrac{1}{(\Delta+1)^3} & \text{for } 0 < \Delta < 1 \\ -\dfrac{1}{(\Delta-1)^3} & \text{for } -1 < \Delta < 0. \end{cases} \tag{31}$$

The Laplace differential equation and the first two boundary conditions are sufficient to determine ψ_3 and ζ; the last condition then allows determination of R_3. Indeed, the general solution of (27) satisfying (28) is given by

$$\psi_3 = \sum_{n=0}^{\infty} \frac{A_n P_n(\cos\theta)}{r^{n+1}}, \tag{32}$$

involving Legendre polynomials P_n. Applying the boundary condition (29) implies that

$$\sum_{n=0}^{\infty}(1-n)A_n P_n(\cos\theta) = 2b\,\zeta\,\cos\theta - c\cos^3\theta \tag{33}$$

from which it follows, using the formulae $\cos^3\theta = [3P_1(\cos\theta) + 2P_3(\cos\theta)]/5$ since $P_1(x) = x$ and $P_3(x) = (5x^3 - 3x)/2$, that

$$\zeta = \frac{3c}{10b}, \quad A_3 = \frac{c}{5}, \quad A_n = 0\ (n \neq 1, 3), \quad A_1 \text{ arbitrary}. \tag{34}$$

From the first equality in (34), and using (18) and (31), we find

$$\zeta = -\frac{\text{sign}(\Delta)}{5(1+|\Delta|)},$$

which provides the following two-term expansion for the flame ball centre z_c:

$$z_c = -\Delta(1+|\Delta|) - \frac{\text{sign}(\Delta)}{5(1+|\Delta|)}\epsilon^2 = -\Delta(1+|\Delta|) - \text{sign}(\Delta)e^{\Delta}\frac{1-|\Delta|}{1+|\Delta|}\frac{\epsilon_L^2}{5}. \tag{35}$$

This is the main result we are after, which exhibits the dependence of the flame ball centre on ϵ_L (or ϵ). We emphasise that formula (35) has been derived, and is expected to be valid, in the limit $\epsilon_L \to 0$ with Δ fixed at a non-zero value.[6] In particular, for $\Delta = 1/2$ we have

$$z_c = -\frac{3}{4} - \frac{e^{1/2}}{15}\epsilon_L^2, \tag{36}$$

a case which will be tested against the numerical simulations. In fact, the simulations whose discussion starts in the next section will be compared with the second order expansions for ψ, R and z_c, which are now all available.

Before doing so, we mention that the solution of the $O(\epsilon^3)$ problem can now be completed. This solution is obtained and its implications briefly discussed in Appendix A; in particular it is found that although the shape of the flame ball is modified by the $O(\epsilon^3)$ correction, the thermal energy enclosed within it is not. Finally, we simply record the 3-term expansions obtained, namely,

$$\psi = \frac{1}{r} + \frac{b\,\epsilon^2}{3}\left(\frac{1}{r} + \frac{1}{r^3} - \frac{3\cos^2\theta}{r^3}\right) + \frac{c\,\epsilon^3}{5}\left(-\frac{\cos\theta}{r^2} + \frac{5\cos^3\theta - 3\cos\theta}{2r^4}\right) \tag{37}$$

$$R = 1 + \frac{b\,\epsilon^2}{3}\left(2 - 3\cos^2\theta\right) - \frac{c\,\epsilon^3}{2}\cos\theta\sin^2\theta, \tag{38}$$

in which b and c are functions of Δ given by (18) and (31).

4. Numerical solution of the free boundary problem

4.1. *Formulation and numerical approach*

Looking for axisymmetric solutions, the free boundary problem (9)–(11) can be expressed in terms of the spherical coordinates defined in (19) by

$$\nabla^2\psi = 0 \qquad \text{for } r > R(\theta) \tag{39a}$$

$$\psi = 0 \qquad \text{as } r \to \infty \tag{39b}$$

$$\psi = 1, \quad \frac{\partial\psi}{\partial r} = -\left(1 + \frac{R'^2}{R^2}\right)^{-1/2} \frac{\mathcal{F}\left(z_c + \epsilon_L \mathcal{F}_0^{-1}\, r\cos\theta\right)}{\mathcal{F}_0} \quad \text{at } r = R(\theta), \tag{39c}$$

where the function $\mathcal{F}$ is defined in (11), $\mathcal{F}_0$ is defined in (18) and

$$\nabla^2\psi = \frac{1}{r^2}\frac{\partial}{\partial r}\left(r^2\frac{\partial\psi}{\partial r}\right) + \frac{1}{r^2\sin\theta}\frac{\partial}{\partial\theta}\left(\sin\theta\frac{\partial\psi}{\partial\theta}\right).$$

Note that the free boundary $\partial\Omega$, represented by $r = R(\theta)$, needs to be determined as well as z_c as part of the solution. Note also that we have used (13) to write $\epsilon = \epsilon_L\mathcal{F}_0^{-1}$ under the equidiffusional assumption $l = 0$, which will be adopted henceforth.

To solve the problem numerically, we introduce new coordinates

$$\xi = r - R(\theta), \quad \hat{\theta} = \theta, \tag{40}$$

so as to fix the free boundary at $\xi = 0$. In terms of these, and dropping the hat notation, Equations (39) take the form

$$\nabla^2\psi = 0 \qquad \text{for } \xi > 0 \tag{41a}$$

$$\psi = 0 \qquad \text{as } \xi \to \infty \tag{41b}$$

$$\psi = 1, \quad \frac{\partial \psi}{\partial \xi} = -\left(1 + \frac{R'^2}{R^2}\right)^{-1/2} \frac{\mathcal{F}\left(z_0 + \epsilon_L \mathcal{F}_0^{-1}(\xi + R)\cos\theta\right)}{\mathcal{F}_0} \quad \text{at } \xi = 0, \tag{41c}$$

where

$$\nabla^2 \psi = \left(1 + \frac{R'^2}{(\xi + R)^2}\right) \frac{\partial^2 \psi}{\partial \xi^2} + \frac{1}{(\xi + R)^2} \frac{\partial^2 \psi}{\partial \theta^2} - \frac{2R'}{(\xi + R)^2} \frac{\partial^2 \psi}{\partial \xi \partial \theta} + \left(\frac{2}{\xi + R} - \frac{R' \cos\theta}{(\xi + R)^2 \sin\theta} - \frac{R''}{(\xi + R)^2}\right) \frac{\partial \psi}{\partial \xi} + \frac{\cot\theta}{(\xi + R)^2} \frac{\partial \psi}{\partial \theta}. \tag{42}$$

As an equation for the free boundary $R(\theta)$ we simply require for computational purposes

$$\frac{\partial R}{\partial r} = 0. \tag{43}$$

Due to the assumption that the problem is axisymmetric, we impose the boundary conditions

$$\frac{\partial \psi}{\partial \theta} = \frac{\partial R}{\partial \theta} = 0 \quad \text{at } \theta = 0,\ \theta = \pi. \tag{44}$$

The additional equation needed to compute z_c is taken to correspond to choosing z_c as the midpoint between the intersection points of the symmetry axis with $\partial\Omega$, namely Equation (A2), which we rewrite here for convenience:

$$R(\pi) - R(0) = 0. \tag{45}$$

The problem (41)–(45) is solved numerically using the finite element package COMSOL Multiphysics®, in a rectangular domain (ξ, θ), where $0 \le \xi \le 400\epsilon_L$ and $0 \le \theta \le \pi$. Once the solution has been calculated in the rectangular domain, the results can be plotted using Matlab® in the cross-sectional x–z plane by setting $x = (\xi + R)\sin\theta$ and $z = (\xi + R)\cos\theta$. The domain is covered by a non-uniform grid of approximately 100,000 rectangular elements. The PDEs and auxiliary conditions, after being entered into the software's PDE interface, are transformed using a finite-element discretisation into a set of nonlinear algebraic equations, which are solved using an affine invariant form of the damped Newton method (see e.g. [15]). The solution has been checked to be independent of the mesh; in particular the Dirichlet boundary condition (41b) applicable at $\xi = \infty$ has been applied numerically at $\xi = 400\epsilon_L$ with negligible loss of accuracy, given that the computational domain is large, with radial size 400 times the typical flame ball radius. The same interface and a similar numerical approach are used in the simulations of the finite-β problem presented in Section 5, without repeating there the details related to the software and the numerical method. We note however that the same software has been successfully used and thoroughly tested in several publications on flames, involving diffusion, premixed and triple flames; see [9–11,16].

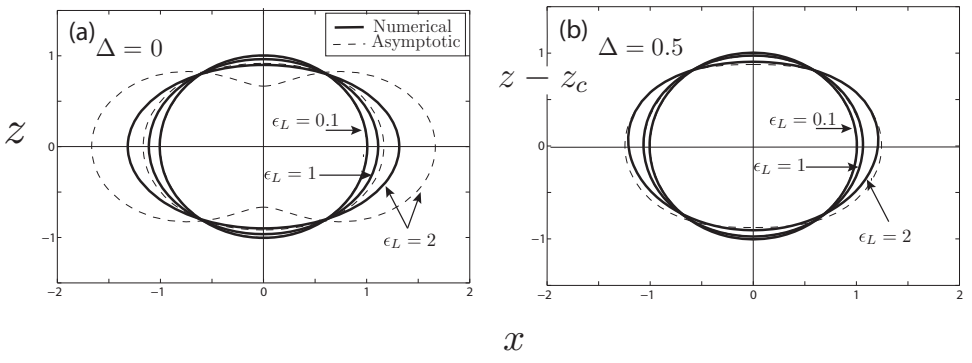

Figure 2. Plots of the flame shape $R(\theta)$ for selected values of ϵ_L, for (a) $\Delta = 0$ and (b) $\Delta = 0.5$. The dashed lines correspond to asymptotic results and the solid lines to numerical computations.

Once the numerical solution has been calculated, the flame ball energy E_B/E_Z can be found by numerically evaluating the formula

$$\frac{E_B}{E_Z} = \frac{3V}{4\pi} \equiv \frac{3}{2}\int_0^{\pi}\int_0^{R(\theta)} r^2 \sin\theta \, \mathrm{d}r \, \mathrm{d}\theta. \tag{46}$$

4.2. *Results*

In this section we present the numerical results corresponding to the problem (41)–(45) and compare them with the asymptotic predictions, namely with the two-term expansions (14), (15), (17) and (36). The main focus is on describing the influence of the parameters ϵ_L and Δ on the flame balls, in particular on the location of their centre z_c, their energy E_B/E_Z, their shape $R(\theta)$ and their maximum radius $R_{\max}$.

4.2.1. *Effect of* ϵ_L

We begin by investigating the effect of ϵ_L on flame balls with a fixed value of Δ. Figure 2(a) compares the asymptotic and numerical flame shapes $R(\theta)$ for selected small to moderate values of ϵ_L in the stoichiometrically balanced case $\Delta = 0$. The figure shows that for low values of ϵ_L there is very good agreement between the asymptotic and the numerics (the curves for $\epsilon_L = 0.1$ are almost indistinguishable). The agreement for small values of ϵ_L is expected because the asymptotic results are derived in the limit $\epsilon_L \to 0$. The agreement remains qualitatively and quantitatively good for $\epsilon_L < 1$. For $\epsilon_L = 2$, however, a qualitative difference can be observed between the asymptotic and numerical flame shapes; the asymptotics predict a strong vertical deflation around the z-axis, which leads in fact to flame breakup for larger values of ϵ_L (not shown). This deflation and breakup are not observed in the numerical solution of the FBP; they simply indicate that the domain of validity of the asymptotics can only be extended to values of ϵ_L close to unity.

We now turn to Figure 2(b), corresponding to $\Delta = 0.5$. It can be seen that the agreement between the numerical and asymptotic solutions is even better in this case; the asymptotic and numerical flame shapes are still indistinguishable for $\epsilon_L = 1$, and there is good agreement between both sets of results even up to $\epsilon_L = 2$. We note that the visible increase

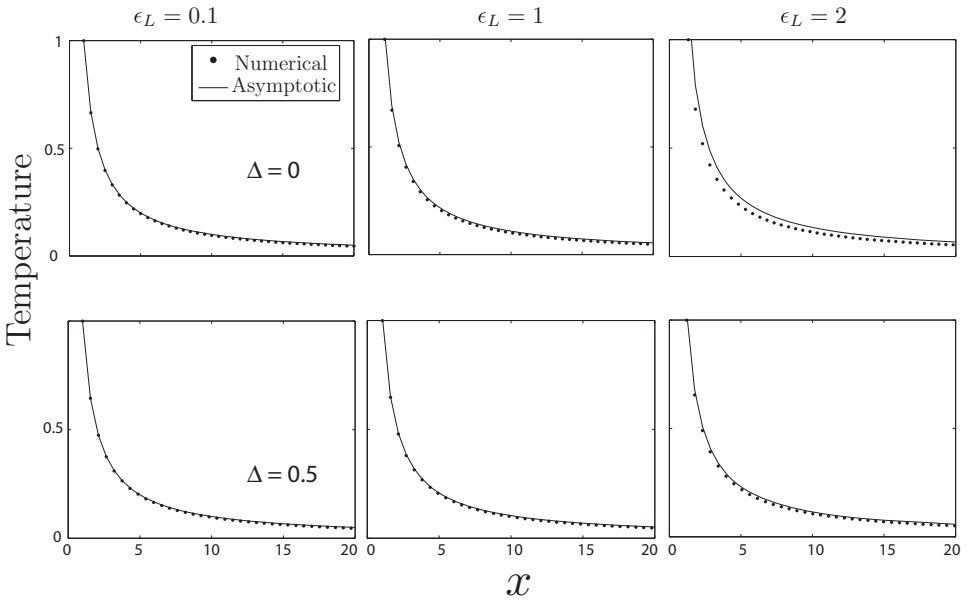

Figure 3. Plots of the temperature ψ in the near field around the flame ball along the line $\theta = \pi/2$ for selected values of ϵ_L and Δ.

in the domain of validity of the asymptotics for the larger value of Δ is in line with the conclusions following Equation (26).

Figure 3 shows a comparison of the asymptotic and numerical solutions for the temperature ψ along the line $\theta = \pi/2$, for selected values of ϵ_L and Δ. The agreement between the asymptotic and the numerical results is seen to be qualitatively good even up to $\epsilon_L = 2$, and quantitatively very good when $\epsilon_L = 0.1$, as expected. Similarly to Figure 4, the agreement is better in the case $\Delta = 0.5$.

In Figure 4 we compare the numerical results for the flame ball energy $E \equiv E_B/E_Z$, calculated using Equation (46), and the maximum radius $R_{\max}$, with the corresponding asymptotic results (17) and (24), for the case $\Delta = 0$. Again, good agreement between the asymptotic and numerical results for low values of ϵ_L can be seen, say up to $\epsilon_L < 0.7$. For larger values of ϵ_L, the numerical values are found to be smaller than the asymptotic ones. The corresponding results for $\Delta = 0.5$ are also given in Figure 6 and show a similar behaviour with an even better agreement.

In Figure 5 the flame ball centre z_c is plotted against ϵ_L for $\Delta = 0.5$ (solid line) with the asymptotic value (horizontal dashed line) obtained from (36); note that no similar figure is needed for the case $\Delta = 0$, for which by symmetry $z_c = 0$ for all values of ϵ_L. The figure shows that there is good agreement for low and moderate values of ϵ_L, say for $\epsilon_L < 1.5$. As ϵ_L increases further, the numerical calculations yield a value of z_c which decreases at a slower rate than the asymptotic value. A full interpretation of the results necessitates the use of (21) with a finite value of β and this point is further discussed in Appendix B. Here, it suffices to take notice of the trend corresponding to $\Delta > 0$, namely that an increase in ϵ_L results in the flame ball centre moving downwards (towards the fuel side) away from the stoichiometric surface (located closer to the oxidiser side, since $\bar{z}_{\rm st} = \Delta > 0$ according to Equation 20).

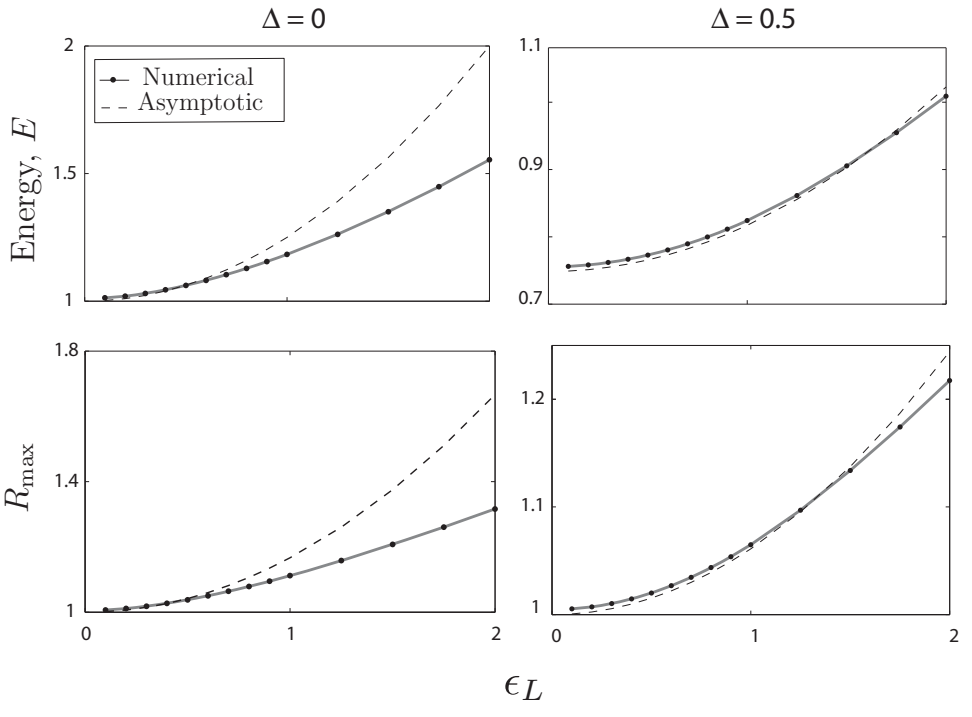

Figure 4. Plots of the flame ball energy, $E \equiv E_B/E_Z$, and the flame ball radius, $R_{\max}$, versus ϵ_L for $\Delta = 0$ and $\Delta = 0.5$.

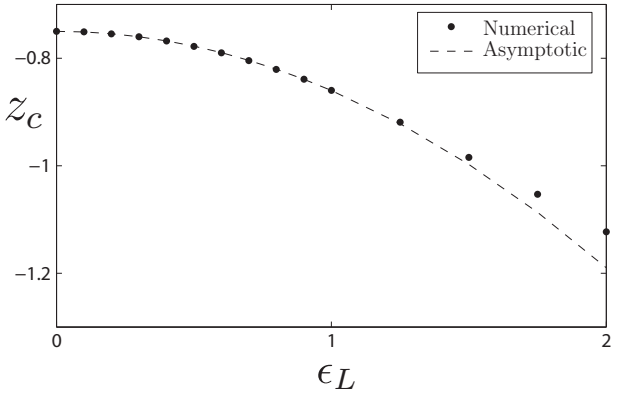

Figure 5. Flame ball centre z_c versus ϵ_L for $\Delta = 0.5$. The dotted line corresponds to the asymptotic formula (36).

The discussion of the last four figures confirms the validity of the asymptotic formulae and indicates their range of applicability. We now provide complementary numerical results for large values of ϵ_L. Shown in Figure 6 are temperature contours around the flame ball (whose shape is represented by a thick line) for selected values of ϵ_L up to a value of $\epsilon_L = 10$, for $\Delta = 0$ and $\Delta = 0.5$. It can be seen that as ϵ_L increases to large values the flame ball becomes thinner in the vertical direction and longer in the horizontal direction, while still remaining roughly elliptical in shape. We note that the asymmetry in the flame shape

observed in the case of $\Delta = 0.5$ is in line qualitatively with the conclusions in the short discussion following (A5) and (A6). The dependence of the flame ball on large values of ϵ_L is further illustrated in Figure 7, where the maximum flame ball radius $R_{\max}$ is plotted versus ϵ_L for large values of ϵ_L, for $\Delta = 0$ and $\Delta = 0.5$. To conclude, we note that solutions to our FBP can be found for arbitrarily large values of ϵ_L (or arbitrarily small values of the Damköhler number); this conclusion is intimately connected and consistent with the

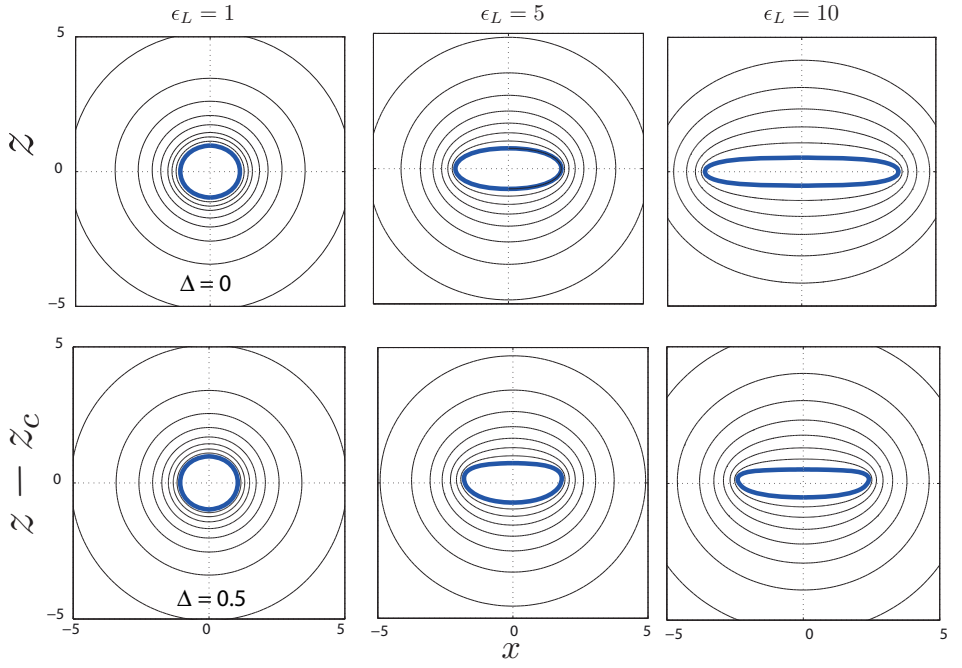

Figure 6. Temperature contours around the flame ball (whose shape is represented by the thick inner line) for selected values of ϵ_L and Δ. The contours are represented by solid lines corresponding to values of ψ decreasing from 1 (the thick inner line) in steps of 0.1.

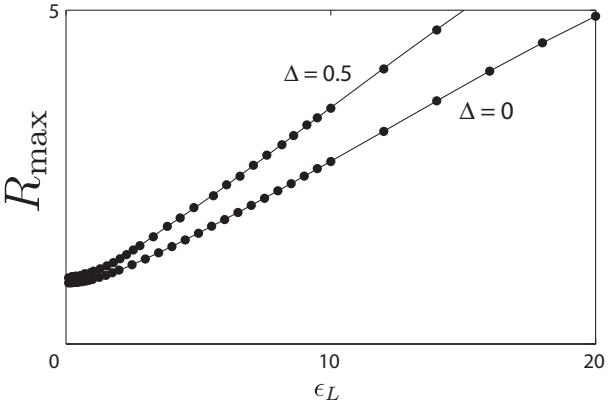

Figure 7. Plots of the maximum flame ball radius $R_{\max}$ versus ϵ_L, for a wide range of ϵ_L, with $\Delta = 0$ and $\Delta = 0.5$.

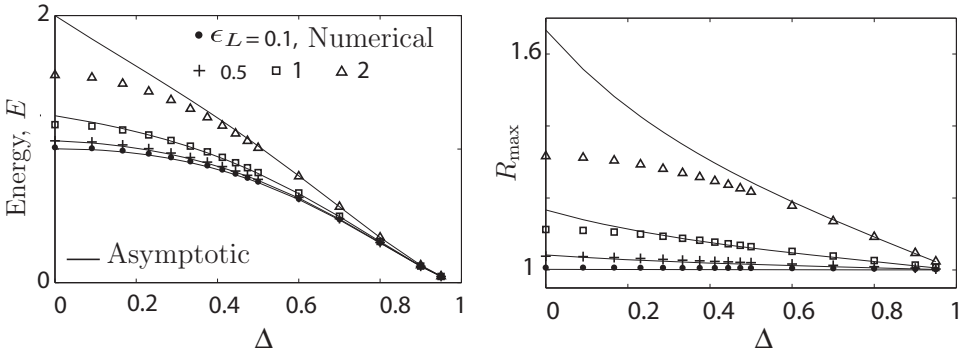

Figure 8. Plots of the flame ball energy $E \equiv E_B/E_Z$ and flame ball maximum radius $R_{\max}$ versus Δ for selected values of ϵ_L. The solid lines correspond to asymptotic results for each of the selected values.

infinite-β limit adopted in the derivation of the FBP. This is an important point which will become clearer in Section 5.4, when we examine the large-β behaviour of the finite-β solutions.

4.2.2. *Effect of* Δ

In this section we examine the influence of Δ on flame balls for fixed values of ϵ_L. Shown in Figure 8 are plots of the flame ball energy E_B/E_Z and its maximum radius $R_{\max}$, corresponding to the asymptotic and the numerical results for selected values of ϵ_L. As expected, very good agreement between the two sets of results is observed when ϵ_L is small enough. For higher values of ϵ_L, better agreement is obtained when Δ is large. This better agreement is consistent with Figure 2, which showed that the flame shapes based on the asymptotics were closer to the numerical flame shapes for $\Delta = 0.5$ than for $\Delta = 0$.

It can also be seen in Figure 8 that, for large values of ϵ_L, the asymptotics overestimate the flame ball energy compared with the numerical results, which curve to lower values as Δ approaches zero; the same is true for the flame ball radius $R_{\max}$.

5. The finite-β problem

5.1. *Formulation*

As stated at the end of Section 2, our main aim is to find stationary solutions to Equations (4) with the boundary conditions (8), focusing on the dependence of their existence domain on the three non-dimensional parameters ϵ_L, Δ and β, with the remaining three non-dimensional parameters identified being assigned the fixed values $\mathrm{Le_F} = 1$, $\mathrm{Le_O} = 1$ and $\alpha = 0.85$. In particular, under the unit Lewis numbers assumption, the equations and boundary conditions imply that $\theta + y_\mathrm{F}$ and $\theta + y_\mathrm{O}$ are known functions of z given by the right-hand sides of (8b) and (8c), respectively. Therefore, a single equation is needed, say the θ equation, in which ω is a function of θ and z. Hence, we have to solve

$$\frac{\partial\theta}{\partial t} = \nabla^2\theta + \frac{\epsilon_L^{-2}\beta^3}{4}\left[1-\theta-\frac{z}{\beta(1-\Delta)}\right]\left[1-\theta+\frac{z}{\beta(1+\Delta)}\right]\exp\left[\frac{\beta(\theta-1)}{1+\alpha(\theta-1)}\right] \tag{47}$$

with

$$\theta = 0 \quad \text{as } x^2 + y^2 \to \infty,\ z \to -\beta(1+\Delta) \text{ or } z \to \beta(1-\Delta). \tag{48}$$

Of course, the stationary axisymmetric solutions to the problem (47)–(48) represent the flame balls in the mixing layer we are interested in. Two other types of solutions of (47) which will be used in our discussion are the one-dimensional diffusion flames $\theta = \theta(z)$ and the two-dimensional travelling-waves $\theta = \theta(x - Ut, z)$, representing triple flames with propagation speed U in the positive x-direction. To obtain these two types of solutions, the boundary condition should be modified respectively to

$$\theta = 0 \text{ as } z \to -\beta(1+\Delta) \text{ or } z \to \beta(1-\Delta) \tag{49}$$

or

$$\theta = 0 \text{ as } x \to \infty,\ z \to -\beta(1+\Delta) \text{ or } z \to \beta(1-\Delta) \text{ and } \theta_x = 0 \text{ as } x \to -\infty. \tag{50}$$

We note that other types of flames also exist in the mixing layer, which include two-dimensional flame tubes (see e.g. [17–19]) which will not be considered herein. They also include expanding flame discs, a structure to which our stationary flame balls may evolve if perturbed (see e.g. Figure 19). The propagation speed of the front of these flames is in fact a function of the disc radius [8–12], and these will not be examined in detail; suffice it to say that their propagation speed is given to a good approximation by that of the 2D triple flames as soon as their radius exceeds a few times L/β.

The numerical approach in the simulations to be presented next is based on the software COMSOL, as discussed at the end of Section 4.1.

5.2. *An illustrative case*

We begin with an illustrative case corresponding to the stoichiometrically balanced case $\Delta = 0$ and $\beta = 10$. Shown in Figure 9 are the reaction rate and temperature fields in the x–z plane for selected values of ϵ_L increasing from left to right. We note by examining the temperature field that the flame ball is practically spherical for small values of ϵ_L and that it becomes more elongated in the horizontal direction as ϵ_L increases.[7] The maximum value of ϵ_L for which stationary solutions exist in this case is found to be $\epsilon_m \approx 2.4$. The flame ball elongation in the horizontal direction is conveniently measured by the maximum flame ball radius $R_{\max}$ introduced in (24) and is plotted in Figure 10. Numerically, $R_{\max}$ is calculated as being the distance between the origin and the location of $\omega_{\max}$, the maximum of ω which is taken in the horizontal plane $z = 0$ in this case where $\Delta = 0$. It is seen that $R_{\max}$ is an increasing function of ϵ_L which diverges to infinity as $\epsilon_L \to \epsilon_m$. Note that, given our choice of the reference length $L_r = L/\beta$, $R_{\max}$ decreases to zero like ϵ_L as $\epsilon_L \to 0$, which is the radius of the Zeldovich flame ball δ_Z, equal to δ_L due to our equidiffusional assumption, scaled (divided) by L_r. The results rescaled by the Zeldovich flame ball radius calculated numerically (in the uniform spherical case) show that the rescaled radius tends to unity as $\epsilon_L \to 0$, as it should.

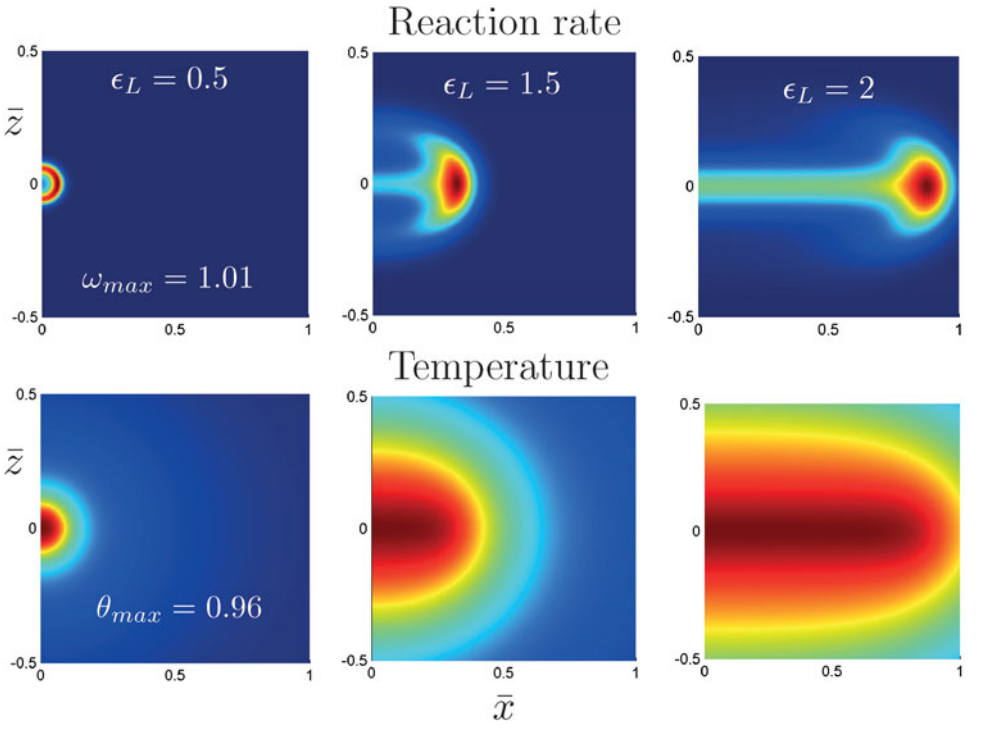

Figure 9. Reaction rate and temperature fields for the (axisymmetric) flame balls in the x–z plane for $\Delta = 0$, $\beta = 10$ and selected values of ϵ_L. Colours vary from blue corresponding to near-zero values to red corresponding to the maximum values indicated. The non-dimensional coordinates $\bar{x}$ and $\bar{z}$ are scaled versions of x and z, as described in the footnote following Equation (5).

We note that a similar behaviour is obtained for other values of β with the main difference being in ϵ_m, the critical value of ϵ_L above which flame balls cease to exist. In fact, ϵ_m is found to be an increasing function of β, as we shall see below.

5.3. *Comparison between the numerical and asymptotic results*

In this section we compare the numerical results of our finite-β problem with the asymptotic results of the FBP summarised in Equations (14)–(17). We start by the stoichiometrically balanced case, $\Delta = 0$, for which Equations (14)–(17) are to be used with $z_0 = 0$, $b = 1/4$, $\mathcal{F}_0 = 1$ and $\epsilon = \epsilon_L$, on account of (18); hence, restricting the asymptotic results to the plane $\theta = \pi/2$ where $R = R_{\max}$, and letting $E \equiv E_B/E_Z$ denote the flame ball thermal energy scaled by that of the Zeldovich flame ball, we have

$$\psi = \frac{1}{r} + \frac{\epsilon_L^2}{12}\left(\frac{1}{r} + \frac{1}{r^3}\right), \quad R_{\max} = 1 + \frac{\epsilon_L^2}{6}, \quad E = 1 + \frac{\epsilon_L^2}{4}. \tag{51}$$

We start by comparing the theoretical predictions for the three quantities listed in (51) with numerical calculations carried out for $\beta = 10$ and $\beta = 20$. The comparison is shown in Figures 11, 12 and 13. As can be seen, the agreement is good for small values of ϵ_L and improves with higher values of β. The agreement is also good when the flame ball

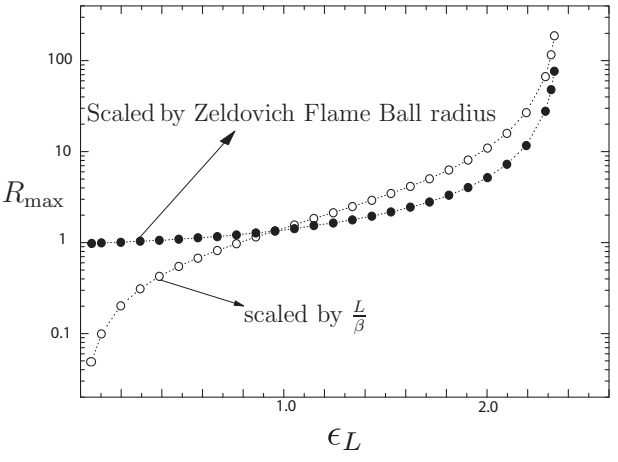

Figure 10. Flame ball maximum radius $R_{\max}$ versus ϵ_L for $\Delta = 0$ and $\beta = 10$.

shape, plotted in Figure 14, which is based on the numerical calculations, is compared with Figure 4 based on the asymptotic and numerical results pertaining to the FBP.

A few additional remarks are useful to explain how some of the numerical results are determined. Specifically, the definition of the flame ball shape, or boundary of the burnt gas domain, used in the computations is based on the temperature contour $\theta = 1 - 2\beta^{-1}$. This is used in evaluating the thermal energy inside the flame ball, defined as the volume integral of θ over the burnt gas domain. This choice, although somewhat arbitrary, is motivated by the fact that this contour passes by the maximum of ω which occurs at the x-axis; this is because the reaction rate ω in the uniform case, also equal to $w(\theta, z = 0)$, attains its maximum at a value of $\theta \sim 1 - 2\beta^{-1}$ as can be checked by a simple calculation.

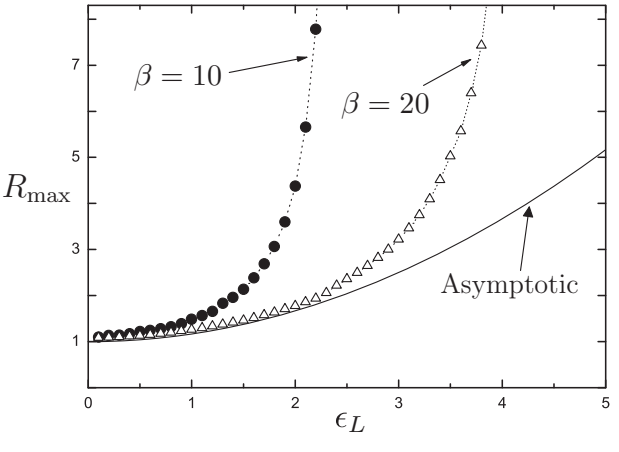

Figure 11. Flame ball maximum radius $R_{\max}$ versus ϵ_L for $\Delta = 0$.

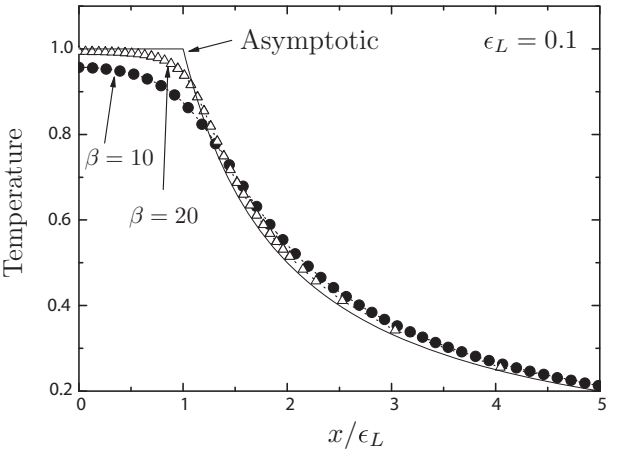

Figure 12. Temperature profile along the x-axis (with x rescaled by ϵ_L).

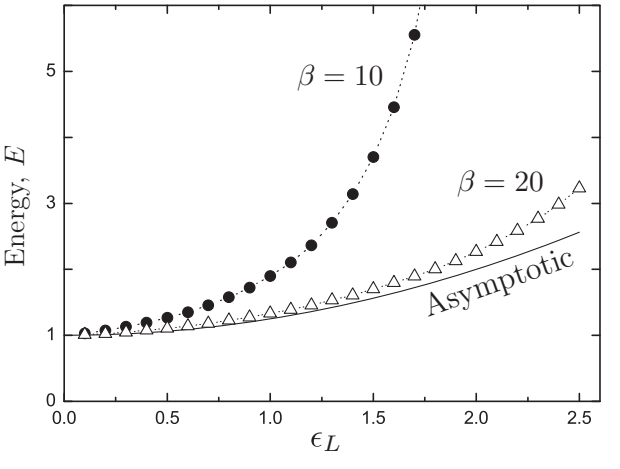

Figure 13. Energy of the flame ball E versus ϵ_L. E is obtained by integrating θ over the domain $\theta > 1 - 2\beta^{-1}$ and rescaling the result by the energy of the Zeldovich flame ball obtained by a similar integration.

5.4. *Existence domain in the β–ϵ_L plane. Relation to triple flames*

From the discussion above, we may conclude that whereas the FBP admits solutions for arbitrarily large values of ϵ_L, stationary solutions for the finite β problem exist only for a restricted range of ϵ_L. For $\Delta = 0$, the domain of existence of flame balls in the β–ϵ_L plane is determined in Figure 15 (left), indicating that ϵ_L must be smaller than a critical value $\epsilon_m(\beta)$, which is an increasing function of β. For comparison, the domain of existence of the two-dimensional triple flames in the mixing layer is shown in the same figure (right). These well studied flames correspond to travelling wave solutions which are illustrated in Figure 16 for selected values of ϵ_L. Their propagation speed U, which can be positive or negative, is plotted versus ϵ_L in Figure 17. It is seen in Figure 15 that the domain of existence of the flame balls coincides, to a good approximation, with that of the positively propagating triple flames. In fact, a more detailed analysis of the numerical results shows that flame

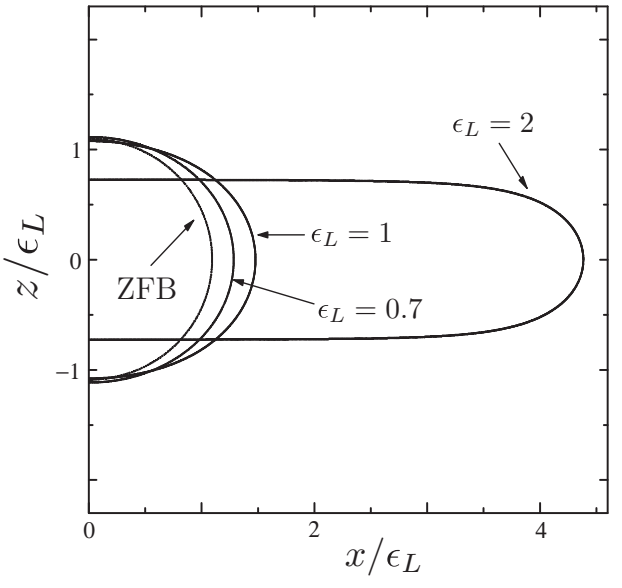

Figure 14. Flame ball shape in the x–z plane, represented by the temperature contour $\theta = 1 - 2\beta^{-1}$ for $\beta = 10$ and selected values of ϵ_L. Also shown is the (spherical) Zeldovich flame ball (ZFB).

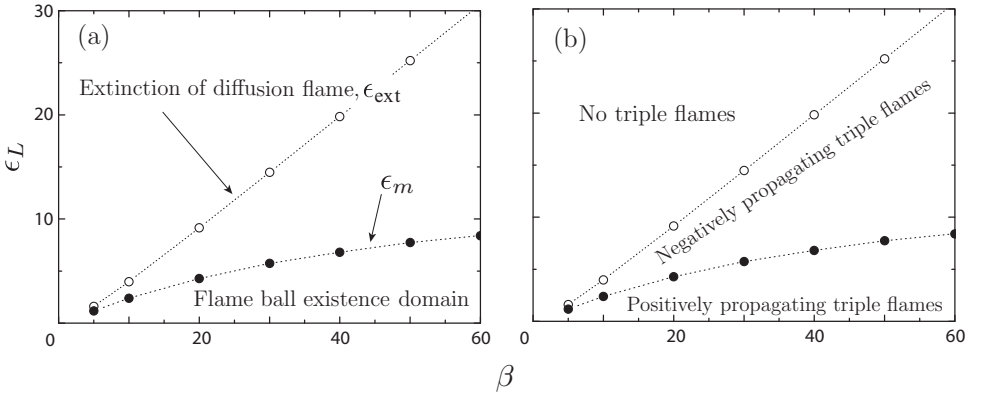

Figure 15. (a) Existence domain of the flame balls in the β–ϵ_L plane. (b) Existence domain of the two-dimensional triple flames ($\Delta = 0$).

balls and positively propagating triple flames exist, in order of magnitude, for $0 < \epsilon < \sqrt{\beta}$, while[8] negatively propagating triple flames exist for $\sqrt{\beta} < \epsilon < \beta$. An order of magnitude argument explaining these scalings for triple flames in a similar (strained mixing layer) configuration can be found in Daou and Liñán [20]. For flame balls, the important point is that the critical value ϵ_m below which these flames exist is found to follow the scaling $\epsilon_m \sim \sqrt{\beta}$. Therefore, in the limit $\beta \to \infty$ under which the FBP is derived, $\epsilon_m \to \infty$, implying that the flame balls are expected to exist for arbitrarily large values of ϵ_L. This is a significant observation as it explains why the FBP admits solutions for all values of ϵ_L, as found in Section 4. Another implication of the scaling found for ϵ_m is that the FBP

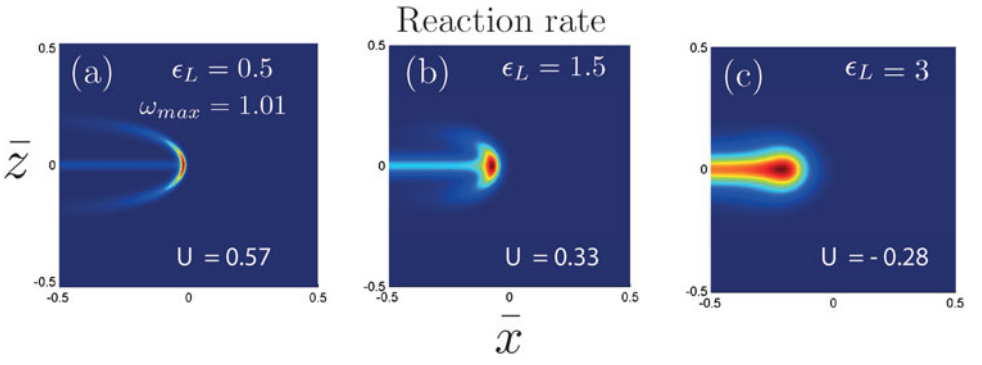

Figure 16. Two-dimensional triple flames in the mixing layer for $\Delta = 0$ and $\beta = 10$. Shown is the reaction rate field for selected values of ϵ_L with the propagation speed U being specified in each case (as indicated in the following figure).

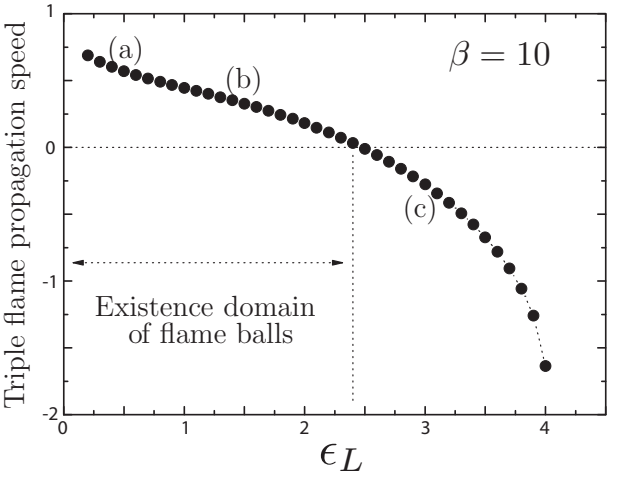

Figure 17. Propagation speed U of the two-dimensional triple flames versus ϵ_L for $\Delta = 0$ and $\beta = 10$. The points (a), (b) and (c) refer to the cases described in the previous figure.

solutions are expected to be a good approximation to the solutions of the finite-β problem provided $\epsilon_L \ll \sqrt{\beta}$.

5.5. *Effect of the stoichiometric coefficient* Δ *on the flame ball existence domain*

Since the stoichiometric coefficient Δ affects the flame balls as well as the planar diffusion flame, it is important to assess the effect of Δ on the existence domain of these structures. This is done in Figure 18 pertaining to a fixed value of β, $\beta = 10$. Plotted versus Δ are the critical value ϵ_m, below which flame balls exist, and the extinction value ϵ_{ext}, below which diffusion flames exist. The figure shows that the existence domain of the flame balls in the Δ–ϵ_L plane (as well as that of the diffusion flame) is practically independent of Δ. This is so except when $\Delta \to 1$; in this limit the flames approach the upper boundary of the mixing layer and their reaction zone structure is affected. This influence of the boundary is however restricted to values of Δ which become closer and closer to one as β is increased

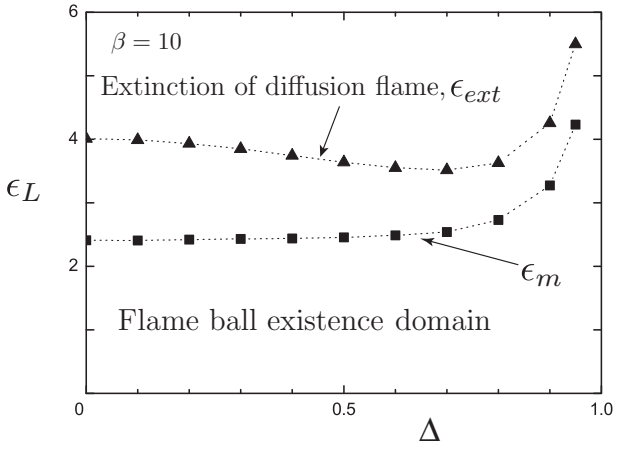

Figure 18. Existence domain of the flame balls ($0 < \epsilon_L < \epsilon_m$) and of the planar diffusion flame ($0 < \epsilon_L < \epsilon_{\text{ext}}$) in the Δ–ϵ_L plane for $\beta = 10$. Note that Δ in the horizontal axis may be replaced by $|\Delta|$.

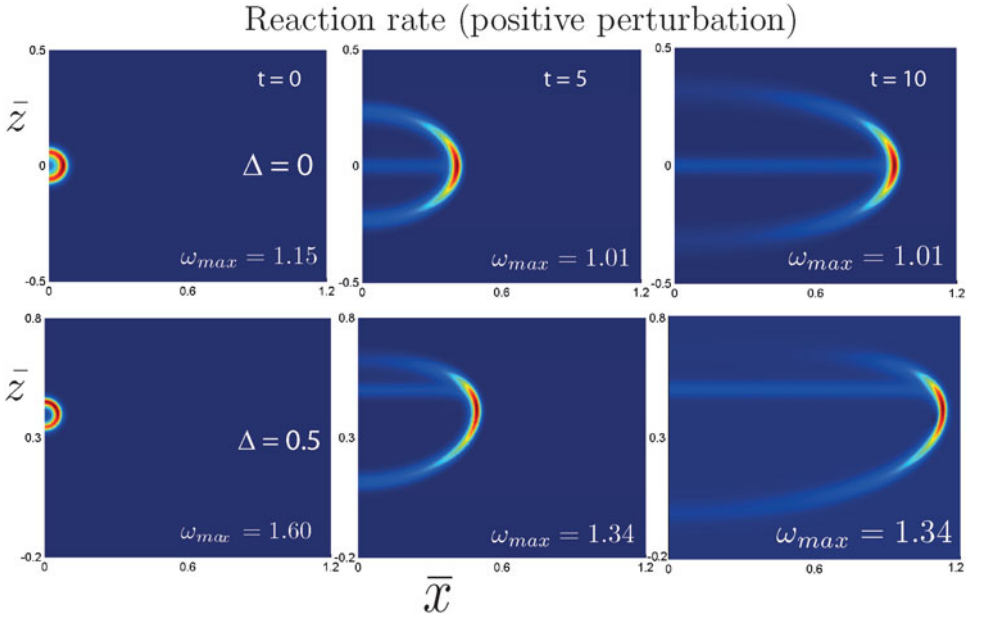

Figure 19. Reaction rate fields at three instants of time for $\Delta = 0$ (top) and $\Delta = 0.5$ (bottom) with $\beta = 10$ and $\epsilon_L = 0.5$. The initial profile used at $t = 0$ corresponds to the stationary flame ball solution to which a localised 'positive perturbation' (increasing the initial thermal energy) is added. Note that the initial quasi-spherical burnt gas region evolves in time as an expanding flame disc in these cases.

(not shown). Note that our computations and diagram have been restricted to those cases for which $\Delta \geq 0$; however, the diagram can be extended to the $\Delta < 0$ cases simply by replacing Δ in the horizontal axis by $|\Delta|$. Finally, we refer the reader to Appendix B for a more thorough discussion of the effect of the stoichiometric coefficient on flame balls.

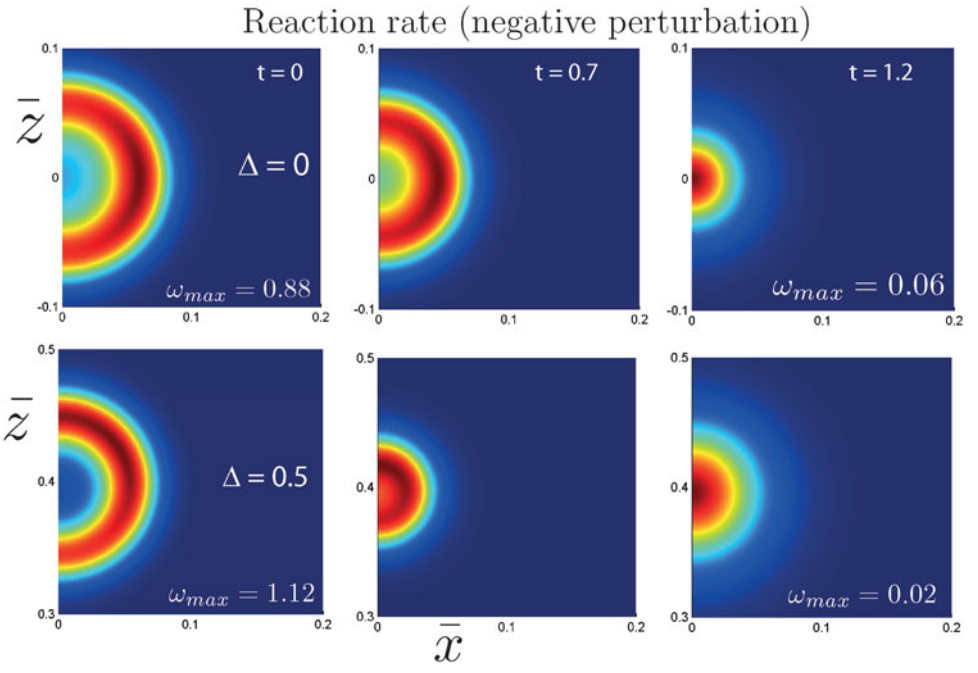

Figure 20. Reaction rate fields at three instants of time for $\Delta = 0$ (top) and $\Delta = 0.5$ (bottom) with $\beta = 10$ and $\epsilon_L = 0.5$. The initial profile used at $t = 0$ corresponds to the stationary flame ball solution to which a localised 'negative perturbation' (decreasing the initial thermal energy) is added.

5.6. *Stability*

Although the stability of the flame balls in the mixing layer is not a main focus in this paper, we provide herein a short confirmation that they are typically unstable. As known from flame ball investigations in uniform premixed mixtures, instability is expected unless additional stabilising effects, combining heat losses and preferential diffusion, are accounted for [3–6]. Therefore, a full stability analysis including such additional effects in non-uniform mixtures will be the subject of a dedicated study. Here we simply illustrate the unstable nature of our stationary solutions by carrying out time-dependent calculations. These are exemplified in Figures 19 and 20, which provide snapshots of the time evolution of the flame in two cases with $\Delta = 0$ and $\Delta = 0.5$. The figures show that a localised perturbation added to the stationary solution can lead either to successful ignition (flame propagation) or to flame extinction. Figure 19 illustrates successful ignition, which typically occurs if the initial perturbation increases the initial thermal energy of the flame ball. Such perturbation (termed 'positive perturbation' in the figure) is seen to result in a propagating triple flame that leaves behind it a one-dimensional diffusion flame. Flame extinction following a 'negative perturbation' is similarly illustrated in Figure 20, where the reported maximum of the reaction rate, $\omega_{\max}$, is seen to decay with time towards zero.

6. Concluding remarks

This paper has been dedicated to the investigation of flame balls in mixing layers and completes a theoretical analysis initiated in [1]. The results are believed to represent a solid basis for understanding and further investigating the problem of forced ignition in

non-uniform mixtures, typically encountered in practical combustion situations involving diffusion flames. Indeed, the thermal energy of the flame balls described and their location in the mixing layer may be argued to represent the minimum ignition energy and the optimal location for its deposition.

Several contributions have been presented in this study. First, an analytical contribution is made by carrying the asymptotic analysis to a higher order. The results thus derived allow to be captured, in particular, the dependence of the location of the flame ball centre on the parameter ϵ_L, i.e. the influence of the Damköhler number ($\sim \epsilon_L^{-2}$) on the optimal ignition location. They also introduce an asymmetry in the flame shape, for non-stoichiometrically balanced mixtures, which is shown to occur without a change in volume, and hence does not affect the minimum ignition energy. Second, two detailed numerical studies of the axisymmetric flame balls are presented for arbitrary values of ϵ_L. The first study addresses the infinite-β FBP and the second one the original finite-β problem based on the constant density reaction–diffusion equations. The validity of the asymptotic formulae of [1] was tested and confirmed by comparison with numerical calculations pertaining to both problems. These calculations, in addition to characterising the range of validity of the asymptotics, provide a fairly complete picture related to the existence and the behaviour of the solutions outside this range. In particular, it is shown that an important difference exists between the infinite-β FBP and the finite-β problem. Indeed, whereas the stationary solutions to the FBP are found to exist for arbitrary values of ϵ_L, those to the finite-β problem are only found in a finite domain of ϵ_L, depending mainly on β and very weakly on the stoichiometric coefficient Δ. Specifically, the ϵ_L-existence domain of the flame balls is found to correspond to $0 < \epsilon_L < \sqrt{\beta}$, in order of magnitude, and to coincide, to a good approximation, with the existence domain of the two-dimensional triple flames with positive propagation speeds in the mixing layer; the latter have negative propagation speeds for $\sqrt{\beta} < \epsilon_L < \beta$, the upper limit characterising the extinction of the one-dimensional diffusion flame. The dependence of the ϵ_L-domain of existence on β exhibited clarifies the reason why the solutions of the FBP exist for arbitrarily large values of ϵ_L. The study also clarifies, for fixed values of β, the combined influence of ϵ_L and Δ on the existence of the flame balls and their location in the mixing layer. This location is also compared with that of the one-dimensional diffusion flame, from which it is found to be able to differ significantly.

Finally we note that the analysis has been restricted to the equidiffusional adiabatic case, in order to understand the rather intricate combined influence of the parameters β, ϵ_L and Δ. In this context, we have provided in passing a quick confirmation of the expected instability of the flame balls, based on time-dependent computations. However, the full stability problem is a crucial one in the context of flame balls [2,21], and will be the subject of a dedicated study allowing the presence of heat losses and non-unit Lewis numbers, as it should [3–6].

Notes

1. It is useful to note that ϵ_L is in fact inversely proportional to the square root of the Damköhler number Da, $\epsilon_L \propto \mathrm{Da}^{-1/2}$, where Da is suitably defined in Equation (6) below.
2. To avoid potential confusion, we note that the non-dimensional model (equations and boundary-conditions) formulated in this section pertains only to flame balls and not to triple or diffusion flames. A few computations of triple and diffusion flames will be needed however in Section 5; there, the necessary modifications of the model will be described succinctly.
3. The reason for this assertion will become clearer later. Indeed, as we shall see, the non-dimensional location of the flame ball centre z_c is determined by the leading order asymptotic

result (12) derived in [1], and the two-term expansion (35) derived in the present paper and checked numerically in Figures 2 and 3.

4. It will be convenient below to use on occasion non-dimensional coordinates based on L, characterised by bars, namely $\bar{x} \equiv X/L$, $\bar{y} \equiv Y/L$ and $\bar{z} \equiv Z/L$. Note that (5) implies that $x = \beta\bar{x}$, $y = \beta\bar{y}$ and $z = \beta(\bar{z} - \bar{z}_{\rm st})$, with $\bar{z}_{\rm st} = \Delta$ according to (2).
5. The non-theoretically-inclined reader may find the material of Section 5 easiest to understand.
6. This formula is not to be used in the limit $\Delta \to 0$ with ϵ_L fixed; clearly the second term is a function of Δ, which is discontinuous at $\Delta = 0$ with distinct right and left limits there. This discontinuity can be traced back to the (finite) discontinuity of the third order derivative $\mathcal{F}_{zzz}(z_0)$ appearing in (31). This occurs in the limit $z_0 \to 0$, corresponding to $\Delta \to 0$, and only in this limit. At any other value of z_0 (the maximum of $\mathcal{F}(z)$ corresponding to a non-zero value of Δ) the function $\mathcal{F}(z)$ is in fact infinitely differentiable.
7. This trend is in agreement with that exhibited by the solutions of the FBP in Figure 6. Note that the diffusion flame seen inside the flame ball when plotting the reaction rate fields for finite β and non-small values of ϵ is absent in the asymptotic model which describes the exterior of the flame ball only; the reaction rate of the diffusion flame inside the ball can be shown indeed to be vanishingly small compared with that of the premixed flame envelope in the limit $\beta \to \infty$ with ϵ_L fixed.
8. Strictly speaking, flame balls and positively propagating triple flames exist for $\epsilon_{\rm ign} < \epsilon < \sqrt{\beta}$, where $\epsilon_{\rm ign}$ corresponds to the ignition of the one-dimensional diffusion flame. However $\epsilon_{\rm ign}$, which strongly decreases with β, is effectively zero; e.g. $\epsilon_{\rm ign} \approx 2 \times 10^{-5}$ for $\beta = 5$ and $\epsilon_{\rm ign} \approx 10^{-11}$ for $\beta = 10$.
9. Similar symmetry arguments can be used below, if needed. For example, a reflection with respect to the vertical axis in Figures B2 and 18 will extend the graphs to negative values of Δ; alternatively, Δ may be replaced by $|\Delta|$.
10. In the finite-β cases, z_c is defined as the barycentre of the one-dimensional region I on the z-axis where the reaction rate is non-negligible ($\omega > 10^{-4}$); specifically, $z_c = \int_I z\,{\rm d}z / \int_I {\rm d}z$. This definition is used because it is consistent with that adopted in the infinite-β FBP.

References

[1] J. Daou and R. Daou, *Flame balls in mixing layers*, Combust. Flame 161 (2014), pp. 2015–2024.

[2] Y.B. Zeldovich, G.I. Barenblatt, V. Librovich, and G.M. Makhviladze, *The Mathematical Theory of Combustion and Explosions*, Consultants Bureau, New York, 1985.

[3] J. Buckmaster, G. Joulin, and P. Ronney, *The structure and stability of nonadiabatic flame balls*, Combust. Flame 79(3–4) (1990), pp. 381–392.

[4] J.D. Buckmaster, G. Joulin, and P.D. Ronney, *The structure and stability of nonadiabatic flame balls: II. Effects of far-field losses*, Combust. Flame 84(3–4) (1991), pp. 411–422.

[5] G. Joulin and J. Buckmaster, *Influence of boundary losses on structure and dynamics of flame-balls*, Combust. Sci. Technol. 89(1) (1984), pp. 57–69.

[6] J. Daou, F. Al-Malki, and P. Ronney, *Generalized flame balls*, Combust. Theory Model. 13 (2009), pp. 269–294.

[7] G. Joulin, *Point-source initiation of lean spherical flames of light reactants: An asymptotic theory*, Combust. Sci. Technol. 43 (1985), pp. 99–113.

[8] J. Buckmaster and T. Jackson, *Holes in flames, flame isolas, and flame edges*, Proc. Combust. Inst. 28 (2000), pp. 1957–1964.

[9] F. Al-Malki and J. Daou, *Triple-flame propagation against a Poiseuille flow in a channel with porous walls*, Combust. Theory Model. (2013), pp. 1–20.

[10] P. Pearce and J. Daou, *Rayleigh–Bénard instability generated by a diffusion flame*, J. Fluid Mech. 736 (2013), pp. 464–494.

[11] P. Pearce and J. Daou, *The effect of gravity and thermal expansion on the propagation of a triple flame in a horizontal channel*, Combust. Flame 160 (2013), pp. 2800–2809.

[12] Z. Lu and S. Ghosal, *Flame holes and flame disks on the surface of a diffusion flame*, J. Fluid Mech. 513 (2004), pp. 287–307.

[13] J.D. Buckmaster and G.S.S. Ludford, *Lectures on Mathematical Combustion*, Vol. 73, SIAM, 1983.
[14] J. Daou, *Asymptotic analysis of flame propagation in weakly-strained mixing layers under a reversible chemical reaction*, Combust. Theory Model. 13 (2009), pp. 189–213.
[15] P. Deuflhard, *A modified Newton method for the solution of ill-conditioned systems of nonlinear equations with application to multiple shooting*, Numerische Mathematik 22 (1974), pp. 289–315.
[16] P. Pearce and J. Daou, *Taylor dispersion and thermal expansion effects on flame propagation in a narrow channel*, J. Fluid Mech. 754 (2014), pp. 161–183.
[17] J. Daou and A. Linán, *Ignition and extinction fronts in counterflowing premixed reactive gases*, Combust. Flame 118 (1999), pp. 479–488.
[18] M. Short, J. Buckmaster, and S. Kochevets, *Edge-flames and sublimit hydrogen combustion*, Combust. Flame 125 (2001), pp. 893–905.
[19] R. Thatcher and J. Dold, *Edges of flames that do not exist: Flame-edge dynamics in a non-premixed counterflow*, Combust. Theory Model. 4 (2000), pp. 435–457.
[20] J. Daou and A. Linán, *The role of unequal diffusivities in ignition and extinction fronts in strained mixing layers*, Combust. Theory Model. 2 (1998), pp. 449–477.
[21] B. Deshaies and G. Joulin, *On the initiation of a spherical flame kernel*, Combust. Sci. Technol. 37(3–4) (1984), pp. 99–116.

Appendix A. Solution of the FBP to $O(\epsilon^3)$

In this appendix we shall complete the solution of the $O(\epsilon^3)$ problem (27)–(30) and briefly discuss its implications. To this end, we first note that from Equations (32) and (34) we have

$$\psi_3 = \frac{A_1 P_1(\cos\theta)}{r^2} + \frac{c}{5}\frac{P_3(\cos\theta)}{r^4}. \tag{A1}$$

The constant A_1, being undetermined, requires an additional condition for its specification. The required condition follows in fact from a precise definition of the flame ball centre. Specifically, we shall define the centre as the midpoint of the intersection points of the boundary $\partial\Omega$ (the flame ball reaction surface) with the symmetry axis. This definition is equivalent to the requirement that $R(\theta)$ satisfies

$$R(0) = R(\pi). \tag{A2}$$

From this equation it follows that $R_3(0) = R_3(\pi)$, that is, on using (30),

$$\psi_3(1, 0) = \psi_3(1, \pi).$$

Applying this condition to (A1) implies that $A_1 = -c/5$ and hence

$$\psi_3 = \frac{c}{5}\left(-\frac{\cos\theta}{r^2} + \frac{5\cos^3\theta - 3\cos\theta}{2r^4}\right). \tag{A3}$$

Evaluating (A3) at $r = 1$ and referring to (30) again we then have

$$R_3 = -\frac{c}{2}\cos\theta\sin^2\theta.$$

The solution of the $O(\epsilon^3)$ problem is now complete and is given by the expansions

$$\psi = \frac{1}{r} + \frac{b\,\epsilon^2}{3}\left(\frac{1}{r} + \frac{1}{r^3} - \frac{3\cos^2\theta}{r^3}\right) + \frac{c\,\epsilon^3}{5}\left(-\frac{\cos\theta}{r^2} + \frac{5\cos^3\theta - 3\cos\theta}{2r^4}\right) \tag{A4}$$

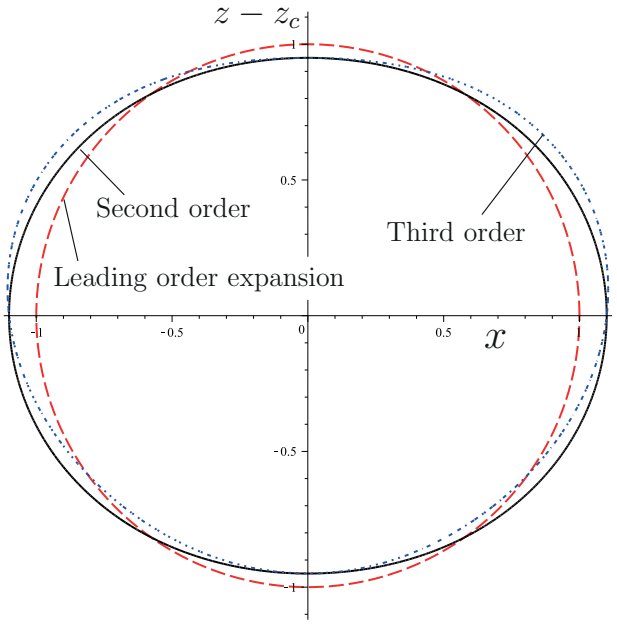

Figure A1. Flame ball shape in the x–z plane for $\Delta = 0.5$ and $\epsilon = 0.95$ based on the leading order, second order and third order expansions for $R(\theta)$.

$$R = 1 + \frac{b\,\epsilon^2}{3}\left(2 - 3\cos^2\theta\right) - \frac{c\,\epsilon^3}{2}\cos\theta\sin^2\theta, \tag{A5}$$

in which b and c are functions of Δ given by (18) and (31). A notable feature of (A5) is that its last term introduces an asymmetry in the flame shape $R(\theta)$ with respect to the plane $\theta = \pi/2$. This asymmetry is however weak, being of order ϵ^3; furthermore it does not modify the volume of the flame ball V (and hence of the thermal energy enclosed within) because the third order term has zero contribution when computing the integral

$$V \equiv 2\pi \int_0^{\pi} \int_0^{R(\theta)} r^2 \sin\theta \,\mathrm{d}r\,\mathrm{d}\theta. \tag{A6}$$

A visual illustration of this asymmetry without change in volume and of the contribution of the three terms in the expansion (A5) to the flame shape is provided in Figure A1. It is seen in this case, pertaining to a positive value of Δ, that the flame becomes more flattened near the upper pole ($\theta = 0$) when the third order term is accounted for; a change in the sign of Δ would simply lead to flame flattening near the lower pole ($\theta = \pi$, not shown).

Appendix B. Stoichiometric effects

In this appendix, we examine the influence of the stoichiometric coefficient Δ on flame balls. We begin by testing the asymptotic prediction that the location of the flame ball centre for $\epsilon_L \to 0$ follows formulae (22) and (23); the formulae indicate that $\bar{z}_0$ is equal to the stoichiometric location $\bar{z}_{\mathrm{st}}$ for $\Delta = 0$ and deviates from it by an amount increasing with Δ to a maximum value approaching $2\beta^{-1}$ as $\Delta \to 1$. This trend is indeed confirmed qualitatively and quantitatively by the finite-β simulations reported in Figure B1. Note that we have restricted the computations to positive values of Δ; the

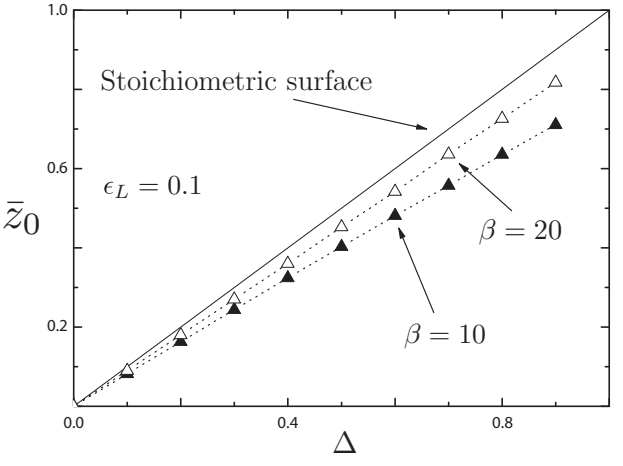

Figure B1. Location of the flame ball centre, $\bar{z}_0$, and location of the stoichiometric surface, $\bar{z}_{\rm st} \equiv \Delta$, versus the stoichiometric coefficient Δ. The simulations pertain to two cases corresponding to $\beta = 10$ and $\beta = 20$ with $\epsilon_L = 0.1$.

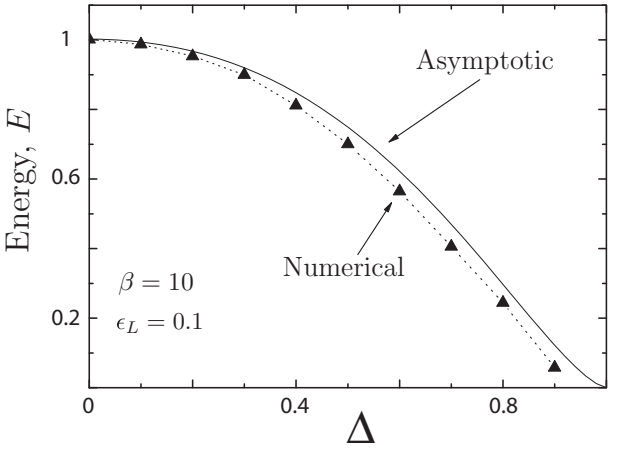

Figure B2. Flame ball energy (defined as in Figure 15) versus Δ (or $|\Delta|$) for $\epsilon_L = 0.1$ and $\beta = 10$.

graph can be extended to negative values using a reflection with respect to the origin given that $\bar{z}_0$ and $\bar{z}_{\rm st}$ are expected to be odd functions of Δ.[9]

In Figure B2, we compare the flame ball energy $E \equiv E_B/E_Z$ predicted by formula (17) with that found numerically. The agreement is quite good for $\beta = 10$ and is even better for $\beta = 20$ (not shown). Note that E decreases from unity as Δ (or more generally $|\Delta|$) increases from zero (the stoichiometrically balanced case); this indicates that the minimum energy required for ignition in the mixing layer is less than that required for igniting a uniform mixture under the conditions prevailing at the stoichiometric surface. Therefore, the figure determines, together with the previous one, both the minimum energy required and the optimum location where it must be deposited, for successful ignition to occur. The results displayed are typical of cases corresponding to small values of ϵ_L.

We now examine the dependence of the location of the flame ball centre (the optimum ignition location) on the value of ϵ_L in a non-stoichiometrically balanced case, say $\Delta = 0.5$ (for $\Delta = 0$ the flame ball and the stoichiometric location are of course always located at $\bar{z} = 0$). Plotted in Figure 3 is the coordinate z_c of the flame ball centre as predicted by the asymptotic formula (36) as well as

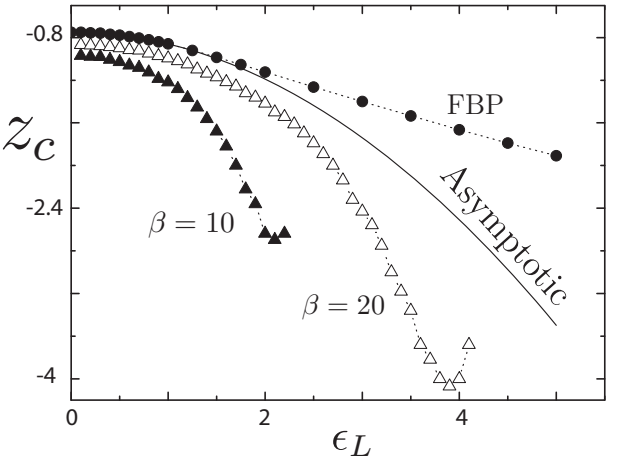

Figure B3. Flame ball centre z_c versus ϵ_L for $\Delta = 0.5$ as predicted by the asymptotic formula (36) and by three numerical simulations. The simulations correspond to the infinite-β FBP and to the finite-β problem with $\beta = 10$ and $\beta = 20$.

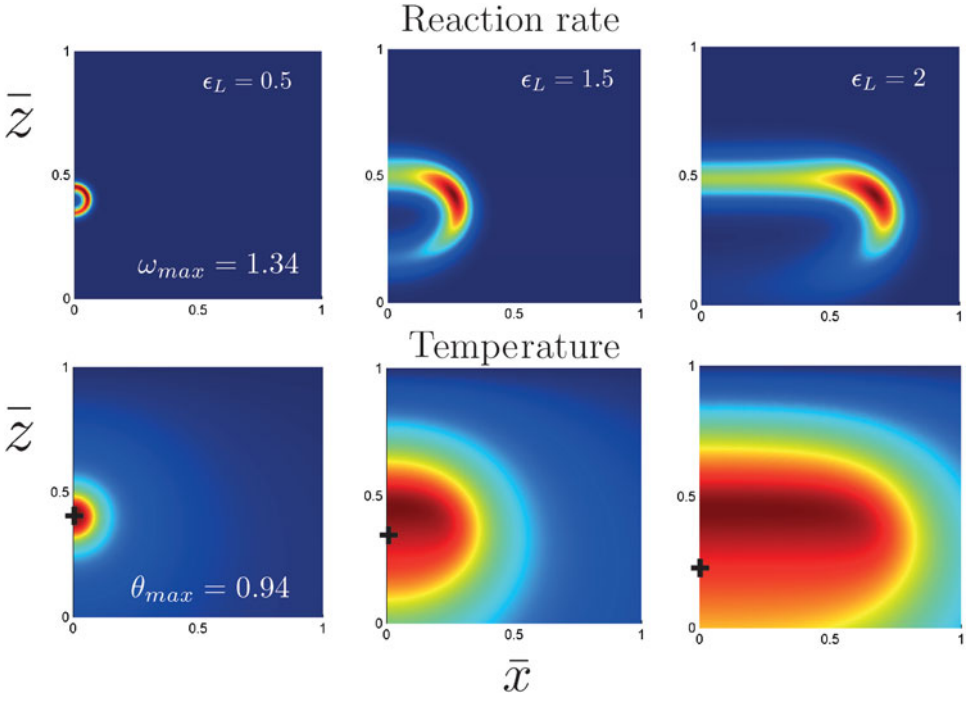

Figure B4. Reaction rate and temperature fields of the (axisymmetric) flame balls in the x–z plane for $\Delta = 0.5$, $\beta = 10$ and selected values of ϵ_L. Colours vary from blue, corresponding to near-zero values, to red, corresponding to the maximum values. The location $\bar{z}_c$ of the flame ball centre is indicated by a '+' sign in the burnt gas.

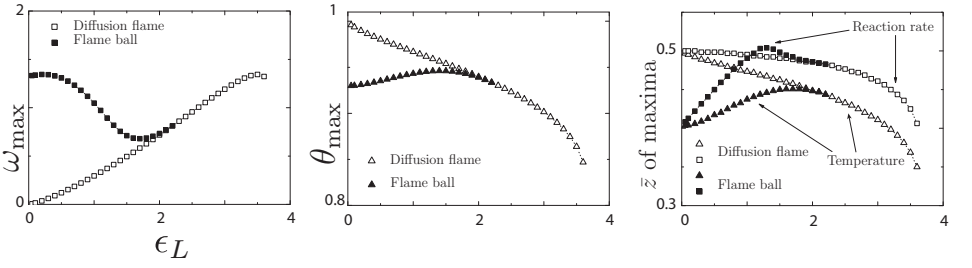

Figure B5. Maximum at the symmetry axis of the reaction rate, $\omega_{\max}$, and temperature, $\theta_{\max}$, for the FB and their locations $\bar{z}$. These are plotted with the corresponding quantities for the planar diffusion flame versus ϵ_L for $\Delta = 0.5$ and $\beta = 10$.

by three numerical simulations; the simulations correspond to the infinite-β FBP and to the finite-β problem with $\beta = 10$ and $\beta = 20$, respectively.[10] As can be seen, the finite-β results are consistent with both the numerical results of the FBP (with an improved quantitative agreement for higher values of β) and with the asymptotic predictions for small-to-moderate values of ϵ_L. All curves predict a monotonic decrease of z_c with increasing ϵ_L, except in a small interval of ϵ_L in the case of the finite-β simulations. This small interval is close to the critical existence value ϵ_m introduced in Section 5.2; in fact, as ϵ_L approaches ϵ_m the flame ball becomes so elongated that it makes the conditions near the symmetry axis approach those of the planar diffusion flame, which are quite different from those corresponding to the infinite-β flame ball solutions, as discussed further below. However, outside this ϵ_L-interval near ϵ_m, the influence of ϵ_L on the flame ball location is satisfactorily described, at least qualitatively, by the infinite-β solutions. More precisely, the fact that z_c appears as a negative decreasing function of ϵ_L implies that an increase in ϵ_L will increase the distance between the flame ball centre $\bar{z}_c$ and the stoichiometric location $\bar{z}_{\rm st} = \Delta$; this is because $\bar{z}_c = \bar{z}_{\rm st} + z_c/\beta$ according to (21). A visual illustration is provided in Figure B4, where the reaction rate and the temperature fields are plotted for three selected values of ϵ_L. In this case the stoichiometric surface is located at $\bar{z}_{\rm st} = 0.5$. The location of the flame ball centre based on Figure B3 is also indicated by a plus sign placed in the burnt gas and is seen to move downwards, away from the stoichiometric location, as ϵ_L is increased.

We close this section by emphasising the difference between the conditions near the symmetry axis for the stationary flame ball solutions and those corresponding to the planar diffusion flame in the mixing layer. This is illustrated in Figure B5, which uses the same parameters as Figure B4. Plotted are the maxima of the reaction rate and temperature for the flame ball at the symmetry axis along with their locations; also plotted are the corresponding quantities for the planar diffusion flame. It is seen that the maxima and their locations are quite different for these two types of stationary flames, especially for small values of ϵ_L. Therefore, adopting the planar diffusion flame conditions as boundary conditions for the flame balls to be anchored near the symmetry axis, as done in [8], is a questionable approximation. We note however that, as ϵ_L is increased towards ϵ_m, corresponding quantities merge with the elongation of the flame ball forcing the conditions at the symmetry axis to be effectively those of the planar diffusion flame. It is in a small neighbourhood of ϵ_m, as mentioned in the discussion of Figure B3 above, that an increase in z_c versus ϵ_L is noted. Examination of additional numerical results (not shown) indicate that the reaction rate at the symmetry axis has three local maxima for moderately small values of ϵ_L (reminiscent of the three branches of a triple flame), the global of which is plotted in Figure B5. As ϵ_L is increased, the middle maximum, corresponding to a diffusion flame, increases in magnitude and tends to merge with the upper maximum. A further increase in ϵ_L results in a decrease in the magnitude of the lower maximum until the lower branch is extinguished near the axis. The increase of z_c with increasing ϵ_L observed in Figure B3 coincides with this extinction of the lower (premixed) branch.